POLITECNICO DI MILANO
School of Civil, Environmental and Land Management Engineering
Master of Science in Civil Engineering for Risk Mitigation

FUSION OF SAR & OPTICAL IMAGERY FOR FLOOD MONITORING

Supervisor: Prof. Dr. Daniela Carrion

Master Graduation Thesis by:
Ameera Ibrahim
Student ID: 905452

ABSTRACT

Disasters, whether natural or man-made have become an issue of mounting concern all over the world. Natural disasters such as floods, earthquakes, landslides, cyclones, tsunamis and volcanic eruptions are phenomena that have devastating effects on infrastructure and property and often result in the loss of human lives. Floods are amongst the most prevalent natural disasters. The frequency with which floods occur, their magnitude, extent and the cost of damage are escalating all around the globe.

Crisis Mapping of inundated regions is crucial for determining the flood extent, to plan the deployment of emergency response teams, and assessment of damages. The main aim of the thesis is to investigate flood mapping using Sentinel-1 and Sentinel-2. The presented method aims to improve the flood classification results from SAR and Optical Imagery by fusing them to limit the disadvantages in both types of imagery and in a way to complement each other when they are processed to obtain a better flood inundation map. The main objective of the thesis is an assessment of the influence of fusing SAR and Optical Imagery on flood classification accuracy.

Two study cases have been considered. The results obtained from confusion matrices indicate enhancement in Overall Accuracy of ~5% and User's Accuracy of more than 24%, for the considered study cases.

Keywords: Natural disasters; Crisis mapping; Floods; Flood Mapping; Flood Classification; SAR; Optical Imagery

RIASSUNTO

I disastri, naturali o provocati dall'uomo, sono una ragione di crescente preoccupazione in tutto il mondo. I disastri naturali come alluvioni, terremoti, frane, cicloni, tsunami ed eruzioni vulcaniche sono fenomeni che hanno effetti devastanti su infrastrutture e proprietà e spesso provocano la perdita di vite umane. Le alluvioni sono tra i disastri naturali più diffusi. La frequenza con cui si verificano le alluvioni, la loro entità, l'estensione e i danni stanno aumentando in tutto il mondo.

La realizzazione di carte di emergenza delle regioni inondate è fondamentale per determinare l'estensione delle alluvioni e permettere il dispiegamento di squadre di pronto intervento e la valutazione dei danni. Lo scopo principale della tesi è indagare la mappatura delle alluvioni utilizzando Sentinel-1 e Sentinel-2. Il metodo presentato mira a migliorare i risultati della classificazione delle alluvioni da SAR e immagini ottiche fondendoli insieme per limitare gli svantaggi in entrambi i tipi di immagini e in modo da completarsi a vicenda. L'obiettivo principale della tesi è una valutazione dell'effeto della fusione di SAR e immagini ottiche sull'accuratezza della mappatura delle alluvioni.

Sono stati analizzati due casi di studio. I risultati ottenuti indicano un miglioramento nell'accuratezza complessiva di ~ 5% e di oltre il 24% nell'accuratezza dell'utente per i casi di studio considerati.

Parole chiave: disastri naturali; Carte di emergenza; Alluvioni; Classificazione; SAR; Immagini ottiche

ACKNOWLEDGEMENT

Throughout the writing of this dissertation, I have received a great deal of support and assistance starting from GOD for helping me join ‘Politecnico Di Milano’ to extend my knowledge and experience with success.

I would like to express my special thanks of gratitude to my supervisor, Prof. Daniela Carrion, who was willing to give me the opportunity to work under her guidance, who shared her expertise, knowledge and gave her valuable time all the way through the study.

I would like to express my love and gratitude to my parents, my sisters, my friends and colleagues who have been motivating me and supporting me throughout the journey and who without their support could not have completed my thesis.

Lastly, I am obliged to Politecnico Di Milano for giving me the opportunity and a wonderful environment to learn, grow and glow.

Table of Contents

LIST OF FIGURES

LIST OF TABLES

List of Abbreviations

RS – Remote Sensing

GIS - Geographic Information System

RADAR - Radio Detection and Ranging

MSI - Multispectral image

SAR - Synthetic Aperture Radar

NIR - Near Infrared Band

SWIR - Shortwave Infrared Band

LiDAR - Light Detection and Ranging

NDWI- Normalized difference water index

ESA - European Space Agency

SNAP- Sentinel Application Platform

AOI – Area of Interest

RF- Random Forest

DT- Decision Tree

KD KNN - K Dimensional K Nearest Neighbour

1. INTRODUCTION

1.1. PROBLEM STATEMENT

Multi-spectral satellite data are preferred for the estimation of water coverage under cloud-free weather conditions due to their high spectral correlation with the open water surface on the ground and respective mapping accuracy (Irwin, 2017). However, as flood events take place during periods of extended cloud coverage the exploitation of multi-spectral data may become questionable. Thus, space-borne radar data may be the only wide covering real time resource for generating frequently updated inundation maps (Behnamian, 2017).

Flood monitoring in this thesis is done with the aid of SAR and optical Imagery fused together to overcome the disadvantages of both types of imagery making use of their advantages. For adequate management of flood, it is essential to find the most competent way to fuse SAR and optical Imagery to delineate flood and retrieve useful information for risk managers., as well as prove there is enhancement of the results obtained fusing SAR and Optical imagery rather than separately analysing SAR (Sentinel 1) or Optical (Sentinel 2).

By exploring different ways to map the flood extent for two study cases, this work aims to contribute in mapping water inundation fusing optical and SAR imagery. Flood supervised classification using Random Forest machine learning algorithm as well as KD KNN supervised classification techniques have been exploited. The methodology is described in chapter 5 of this thesis.

Error matrices are used to assess classification accuracy. Overall accuracies, user's and producer's accuracies, and the Kappa statistics are derived from the error matrices to determine if there is an enhancement using the introduced methodology.
Specifically, this study aims to answer the Question stated in Research Objectives addressed in the next section of introduction.

1.2. RESEARCH OBJECTIVES

The Overall objective of my thesis is to experiment the quality and results obtained from the fusion of SAR and optical imagery that could improve flood mapping.

This research will be guided by the following questions:

Research question 1:

Does the use of the fused SAR and Optical data improve flood mapping in different areas in comparison to existing approach of analysing each data separately?

To answer the first question, the data are fused and classified to extract the flooded area and the results are validated against the reference made from one of the data sources provided by Copernicus as well as the fused image to conclude the quality and improvement of the results or otherwise.

Research question 2:

What is the influence of parameters on classification accuracy?

High classification accuracy is often a goal for researchers. One of the objectives of this research is observe the change in the classification accuracy of flood mapping experimenting different kind of classification algorithm as well as working with the training sample and different bands of SAR and Optical data to achieve a better solution for flood monitoring.

Computing confusion matrices on these multiple classification algorithms will help to determine their influence on the classification accuracy.

Research question 3:

What are the uncertainties and limitations of this approach?

Every technique of image processing carries some uncertainties and limitations. The approach described in this thesis will encounter them as well. Each step in the methodology will address this third research question. Aspects which might be expected to lead to uncertainties are as follows:

- Long Processing Time,
- Memory Deficiency,
- Data Quality
- Lack of Specific Available Data And
- Influence of Environment.

1.3. THESIS OUTLINE

This thesis has been organized into 5 chapters.

Chapter 1 Presents the introduction, the aim of the thesis and defines the objective of the thesis.

Chapter 2 Presents floods criticality and statistics.

Chapter 3 Presents a literature review on the State of Art on flood monitoring using different methods.

Chapter 4 Presents the study area, the data source and data processing.

Chapter 5 Presents the methodology and approach employed for this research.

Chapter 6 Presents the results, the conclusion and future work.

2. FLOODS EVENTS AND FLOOD MAPPING

2.1. FLOODS

Floods are one of the most common widespread natural hazards with global average annual flood loss estimated to US$ 104 billion (UNISDR, 1996 - 2015). Additionally, as can be seen in Figure 1 (UNISDR, 1996 - 2015) the frequency of occurrence of floods is much higher than other disasters. In years 1995–2015, floods were estimated to represent 43% of all weather-related catastrophes, reaching more than 3,000 documented flood disasters, affecting 2 to 3 billion people, with a total of 157,000 fatal casualties. Their widespread existence, frequency with which floods occur, their magnitude, extent and the cost of damage and destruction drives scientists to investigate this phenomenon thoroughly (Berz, 2001; Schumann, 2015).

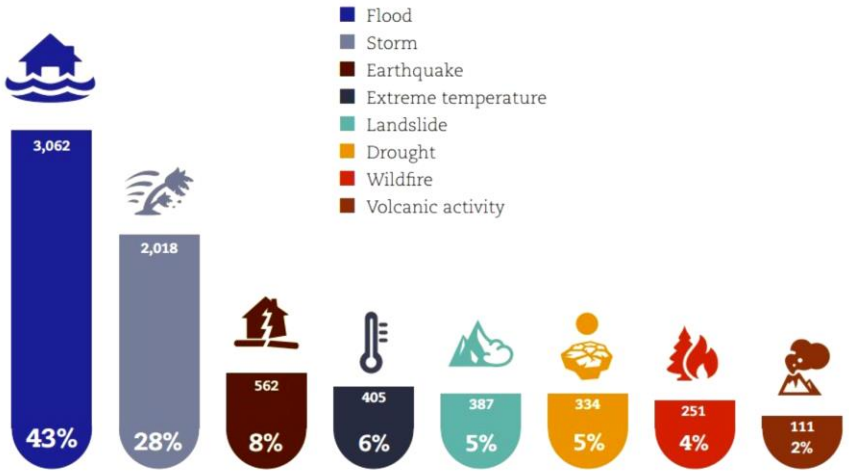

Figure 1: Percentage of occurrences of natural disasters by disaster type in years (UNISDR, 1996 - 2015)

In 2007, the European Commission indicated that floods were natural occurrences which could not be avoided. However, there is a growth in the probability and adverse impacts of flood events due to increase in population and some human activities such as growing human settlements and economic resources in floodplains and a decrease of the natural water reservation by land use coupled with climate change. The sustained climate change will increase the probability of severe, persistent and irreversible consequences. Extreme sea level events and floods will occur more frequently, with severe damages to Europe's coastal communities (European Commission, 2007).

In Europe, detected data suggest that climate change has already significantly changed flood magnitude, timing and extent (Blöschl, G. et al., 2019) . The annual water discharges in Europe have generally been observed to increase in the north and decrease in the south (EEA, 2010; EEA, 2012) , a trend that is predicted to hold in the future, as is linked with probable changes in precipitation regimes that control the intensity and frequency of rain-fed floods and possibly of flash floods (Feyen et al., 2006, 2010).

Most notable increases in flood losses are projected in these regions of Europe (Belgium, Denmark, France, Germany, Ireland, Luxembourg, the Netherlands and the United Kingdom of Great Britain and Northern Ireland), as well as for Hungary and Slovakia (Feyen, 2016) 2010.

The Secretary General of United Nation Quoted *"The COVID-19 pandemic has disrupted lives worldwide. At the same time, the heating of our planet and climate disruption has continued apace. Record heat, ice loss, wildfires, floods and droughts continue to worsen, affecting communities, nations and economies around the world".*

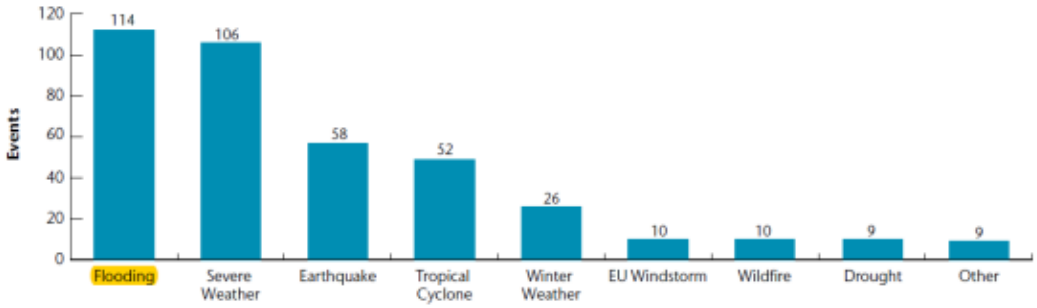

Figure 2: Number of occurrences of each type of natural disaster in 2018 (Podlaha, 2019)

2.2. STATISTICS ABOUT FLOOD IMPACTS

Flooding is a natural phenomenon and is not a rare process associated with river dynamics. Flood has always been a multiplying factor to human's problems throughout the ages, floods have affected human health, the environment, cultural heritage and economic activities and caused many more damages as shown below in Figure 3.

		Measurement	
		Tangible	**Intangible**
Form of damage	**Direct**	Physical damage to assets: - buildings - Contents - Infrastructure	- Loss of life - Health effects - Loss of ecological goods
	Indirect	- Loss of industrial production - Traffic disruption - Emergency costs	- Inconvenience of flood recovery - Increased vulnerability

Figure 3: Classification of the types of damages caused by the flooding (Messner, 2007)

Historical records show that resulting flooding in the arid regions of Somalia and Kenya, malaria outbreaks were reported during the 1997-1998 El Niño event. Subsequently, extensive research on mosquito vectors of Rift Valley Fever in Kenya (mainly Aedes and Culex species) clearly has associated the risk of outbreaks with flooding. (Githeko, A. & Ndegwa, W., 2001)

Following the 1997-1998 El Niño event in East Africa, a Rift Valley Fever outbreak in Somalia and northern Kenya killed up to 80% of livestock and affected their owners (Patz, 1998). In West Africa the disease is linked to epizootic diseases with increased risks during the wet season. During the 1997-1998 El Niño, the rise in sea-surface temperature and excessive flooding (Patz, 1998) provided two conducive factors for cholera epidemics which were observed in Djibouti, Somalia, Kenya, Mozambique and the United Republic of Tanzania, all of which border the Indian Ocean. Cholera epidemics also have been observed in areas surrounding the Great Lakes in the Great Rift Valley region. Between 1991 and 1996 cholera also affected 21 counties in Peru resulting in almost 200000 cases and 11700 deaths (Parmenter, 1999)

Leptospirosis, a disease allied with flooding, is a major concern in some parts of Europe. Outbreaks of the disease have been reported following floods in Ukraine and the Czech Republic in 1997 (Kríz, 1998) and Portugal in 1967 (Simoes, 1967). As well as the direct injuries and infections resulting from flooding, psychological suffering including cases of suicide that has been associated with the event.

Floods can root pollution of public water supplies with both bacteria and parasites as surface discharge flows into rivers and reservoirs. A decrease in the availability of clean water surges the risk of drinking contaminated supplies and also reduces the amount of water available for personal hygiene thus leading to skin infections (WORLD HEALTH ORGANIZATION, 2003).

In the period 1998-2002, there have been more than 100 major floods in Europe (including the 2002 catastrophic floods along the Danube and Elbe rivers) that caused several hundred fatalities, the displacement of about 500,000 people and over € 25 billion in insured economic losses. Until 2009 flooding and storms were still the costliest hazards, and the number of fatalities had reached 1126 in 213 recorded flood events. The overall losses recorded for this period now added up to about EUR 52 billion for floods and EUR 44 billion for storms. (EEA, 2011)

Increases in heavy precipitation events and floods will cause more weather-related accidents, delays, and traffic disturbances in the already congested networks. Additionally, problems like silting, changes in river morphology and damages of banks and flood protection schemes, whereas airports may suffer infrastructure damages and increased delays and cancellations of operations (Christodoulou A., Demirel H, 2018).

Predictions in Europe as a whole that will be more prone to flood risk (with mean annual river flow set to increase), water stress will be more pronounced in Southern European regions, and may well cause tensions between different users of dwindling reservoirs and aquifers. Under 2°C warming, median river flows in Mediterranean regions are expected to fall in all four seasons (EUROPEAN COMMISSION, 2018).

Flooding alone may cost EU countries up to EUR 1 trillion per year in damages by the end of the century. Most of this would be due to coastal flooding (up to EUR 961 billion). Damages from river flooding could also rise to up to EUR 112 billion compared to EUR 5 billion today, and there is considerable increase in river flood risk for Europe even under a 1.5º C warming scenario. This could also affect transport infrastructure. By the end of the century, under a high warming scenario, about 200 airports and 850 seaports of different size across the EU could face the risk of inundation due to higher sea levels and extreme weather events. (EUROPEAN COMMISSION, 2018)

PESETA IV study estimates that currently river flooding causes damage of 7.8 €billion/year in the EU and UK, which is equivalent to around 0.06% of current GDP. Moreover, more than 170,000 people every year are exposed to river flooding (JRC PESETA IV, 2020). Coastal flood losses would grow by two orders of magnitude and climb to 250 €billion/year in 2100, while 2.2 million people would be exposed per year to coastal inundation compared to 100,000 at present

PESETA IV assesses the consequences of climate change for eleven climate impact categories: human mortality from heat and cold waves, windstorms, water resources, droughts, river flooding, coastal flooding, wildfires, habitat loss, forest ecosystems, agriculture and energy supply. Some of the Key findings related to flooding is that if Global warming and continued development in flood prone areas will progressively increase river flood risk. With 3°C global warming by the end of the century, river flood damage in the EU and UK would be six times present losses of 7.8 €billion/year and nearly half a million people would be exposed to river flooding each year, compared to 170,000 now. Keeping global warming with 1.5°C would halve these economic impacts and reduce the number of people exposed by 230,000. (JRC PESETA IV, 2020).

Finally, not only physical health and physical structures are affected by flooding but also there is an increase in the instances of mental illnesses that was also observed among the flood victims especially Post Traumatic Stress Disorder (PTSD), depression, and developing suicidal thoughts (Zhong, 2018).

3. STATE OF ART

Flood risk maps are very useful in preparing for and in mitigating the impact of floods by minimizing the exposure and vulnerability of human lives, property and infrastructure. In recent time, it is becoming increasingly common to use GIS and Remote Sensing for flood delimitation and its attendant risks and hazards (World Meteorological Organization, 2013). During floods, decision makers and rescue workers require rapid and detailed status reports to identify areas affected by the floods, direct rescue missions and implementation of mitigation measures. Remote sensing helps in the quick assessment of flood damage through the provision of comprehensive, rapid, accurate and real time multi temporal imagery with information on what is actually happening on the ground. The previous chapter introduces the negative impact of flood globally and therefore, highlights the importance of flood monitoring to introduce plans for prevention, protection and mitigation. This chapter is dedicated to discuss the state of the art of flood mapping based on remote sensing techniques.

3.1. FLOOD MAPPING USING REMOTE SENSING TECHNIQUES

Remote Sensing has made substantial contribution in flood monitoring and damage assessment that leads the disaster management authorities to contribute significantly. “Remote sensing is the science and art of obtaining information about an object, area, or phenomenon through the analysis of data acquired by a device that is not in contact with the object, area, or phenomenon under investigation” (T. M. Lillesand, R. W. Kiefer and J. W. Chipman, 2008).

Remote sensing is the practice of acquiring information about Earth’s land and water surfaces by using images acquired from an overhead perspective and not by being in contact with the body of interest (Campbell and Wynne, 2011). Remotely sensed satellite observations from the space have fundamentally changed the way in which scientists study the atmosphere, oceans, land, vegetation, glaciers, sea ice, and other environmental aspects of the Earth's surface. Half a century of the satellite observations of the Earth have provided dramatic pictures and they are the basis for a new scientific paradigm: (Horvat, 2012). By utilizing sensors operating in the visible and microwave spectral bands, remote sensing techniques.

The quantities that are measured using remote sensing sensors are the emitted, scattered, and reflected electromagnetic energy from the phenomena under investigation. Useful information is then extracted through interpretation of these measurements (Intera Kenting Ltd, 1992).

The practice began in 1850–1860 as balloonists took ground photographs using the newly invented camera. Aerial photography was used during the First World War and was developed greatly during the Second World War, when German V-2 rockets launched and carried remote sensors into space. Remote sensing matured in the 1970s when the Skylab and Landsat satellites were launched, with the mission of monitoring land and ocean surfaces (Planatek Italia, 2019). The first integration of remote sensing with flood monitoring mentioned in literature dates back to the 1970s, where data from Landsat 1 helped to analyse the Mississippi flood of 1973. The ERTS data provided the first opportunity for mapping the regional extent of flooding at the time of the imagery (Morris Deutsch Fred Ruggles, 1974).

Similarly, many more studies involving mapping of floods and water surfaces were developed using remote sensing. They differ in their applied methods (index-based, thresholding, change detection), spatial resolution, the analysis approach (pixel-based, object-based), sensors used and, most importantly, by main data type - optical, SAR, Digital Elevation Model (DEM), Light Detection and Ranging (LiDAR).

3.2. OPTICAL SATELLITE IMAGERY FOR FLOOD MAPPING

Optical remote sensing is carried out by passive systems that use the sunlight as source to image the Earth's surface. Thus, low solar angles and the atmosphere, especially cloud coverage, hamper useful data acquisitions especially during flooding that is coupled with thick cloud coverage during event occurrence. The spectral acquisition ranges between visible light (VIS) (400 - 700 nm) and near-infrared (NIR) (700 - 1300 nm) or short-wavelength infrared (SWIR) (1300 – 3000 nm) as shown in the figure 4 below (Lillesand, T.M., Kiefer, R.W. & Chipman, J.W.,, 2008). Clouds during the acquisitions reduce the number of available images significantly as with every optical satellite mission.

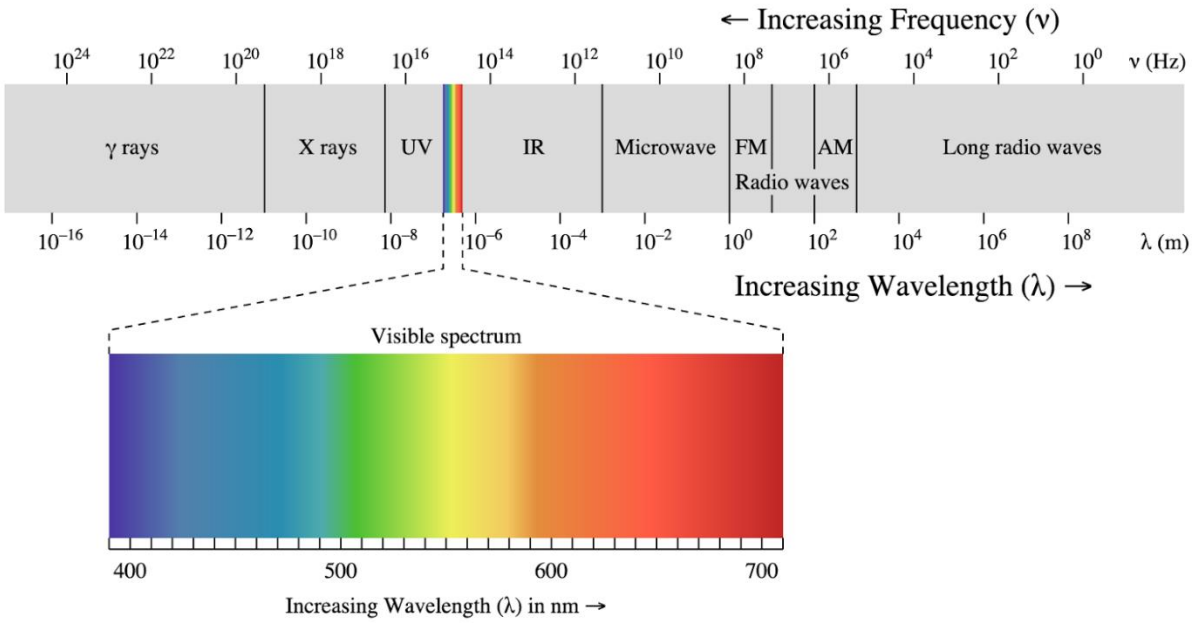

Figure 4: Spectral Wavelength

Earth observation via satellites dates back to the Keyhole-Satellites of the United States (U.S.) Corona-program in the 1960s. After the U.S. government declassified the images from the Corona-program the panchromatic films were digitized and are provided for a small price (Schowengerdt, 2007). Since 1972 the Landsat satellites enable regular multi-spectral acquisition of the Earth's surface. The data base of Landsat archive images is immense and the images are available for free, thus, they have a great potential for long-term lake monitoring (Nath, R.K. & Deb, S.K., 2010) . Landsat images acquire only medium-resolution images, as the spatial coverage is negatively correlated to the spatial resolution.

In 1999 the multi-spectral ASTER sensor was launched on board of the Terra satellite, however, the images have only available been free of charge since April 2016 (Tan, H. & NASA, 2016). The resolution of the ASTER images is 15 m in red, green and NIR, 30 m in SWIR and 90 m in thermal. A blue band is not acquired. ASTER images have proven useful for the monitoring of lakes (Gholizadeh, M., Melesse, A. & Reddi, L.,, 2016).

In the last two decades several commercial satellite missions with a high spatial resolution were launched, e.g., IKONOS, WorldView-2/3, SPOT 5/6/7, Quickbird, and RapidEye (RE). However, a disadvantage of those satellite missions is the cost of the image data and the limited availability of archive data. The high-resolution satellites generally do not acquire the Earth's surface regularly, but only on-demand. RE images which have been acquired since 2009 are available freely for German scientists with a data proposal.

A great potential for Flood monitoring is the new Copernicus Earth observation program: the first high-resolution optical satellite (Sentinel-2a) launched in 2015, and joined by a second satellite Sentinel-2b in 2017, that is identical in construction (Drusch, M. et al.,, 2012). The Sentinel-2 satellites have a spatial resolution of 10 m to 60 m. The multi-spectral images include VIS, red edge, NIR and SWIR and are provided free of charge.

3.2.1. Sentinel 2

Sentinel 2 is the Multispectral optical imagery (MSI) data that was used as a Dataset for the study cases and hence is explained in more details in this section of this thesis.

The Copernicus Sentinel-2 mission MSI works passively, by collecting sunlight reflected from the Earth and comprises a constellation of two polar-orbiting satellites placed in the same sun-synchronous orbit, phased at 180° to each other. It aims at monitoring variability in land surface conditions, and high revisit time (10 days at the equator with one satellite, and 5 days with 2 satellites under cloud-free conditions which results in 2-3 days at mid-latitudes) will support monitoring of Earth's surface changes. Each satellite carries an innovative wide swath high-resolution multispectral imager with 13 spectral bands as shown below in figure5, for a new perspective of our land and vegetation (THE EUROPEAN SPACE AGENCY).

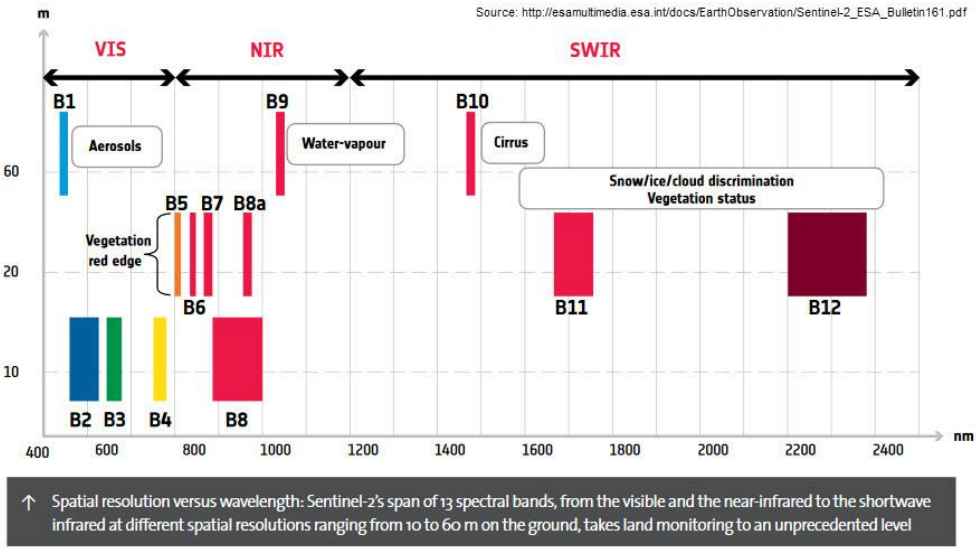

Figure 5: Spectral Bands of Sentinel 2

	Spectral Band	Centre Wavelength (nm)	Band Width (nm)	Spatial Resolution (nm)
B1	Coastal aerosol	443	20	60
B2	Blue (B)	490	65	10
B3	Green (G) [1]	560	35	10
B4	Red (R) [1]	665	30	10
B5	Red-edge 1 (Re1) [1]	705	15	20
B6	Red-edge 2 (Re2) [1]	740	15	20
B7	Red-edge 3 (Re3) [1]	783	20	20
B8	Near infrared (NIR) [1]	842	115	10
B8a	Near infrared narrow (NIRn) [1]	865	20	20
B9	Water vapor	945	20	60
B10	Shortwave infrared/Cirrus	1380	30	60
B11	Shortwave infrared 1 (SWIR1)	1910	90	20
B12	Shortwave infrared 2 (SWIR2)	2190	180	20

Figure 6: Spectral Bands of Sentinel 2 and Specifications

Sentinel-2 mission is the result of close collaboration between the European Space Agency (ESA), the European Commission, industry, service providers, and data users.

Sentinel 2 Specification	
Band	13 bands
Resolutions	Four bands at 10m, six bands at 20m and three bands at 60m spatial resolution.
Revisit time	For each single SENTINEL-2 satellite is 10 days and the combined constellation revisit is 5 days.
Product Levels	Level-0, Level-1A and Level-1B are not made available to Users Level-1C and Level-2A orthorectified UTM/WGS84 projection
Altitude	785 km
Field of View (FOV)	290 km
Launched	Sentinel-2A on 23 June 2015 Sentinel-2B on 7 March 2017
Site	Kourou, French Guiana
Launcher	Vega rocket
Design life	7 years
Tiles	100x100 km2
Tile Projection	UTM/WGS84
Price	Free of Charge upon user registration

Table 1:Sentinel Specification Summary (THE EUROPEAN SPACE AGENCY)

This Sentinel-2 observation data acquired can be utilised by services such as (THE EUROPEAN SPACE AGENCY):

- Land monitoring
- Emergency management
- Security
- Climate change.

Figure 7 shows an infographic which answers questions about Sentinel 2, to understand more about its design, the main applications it could be used in, to whom the services are offered and when was it launched.

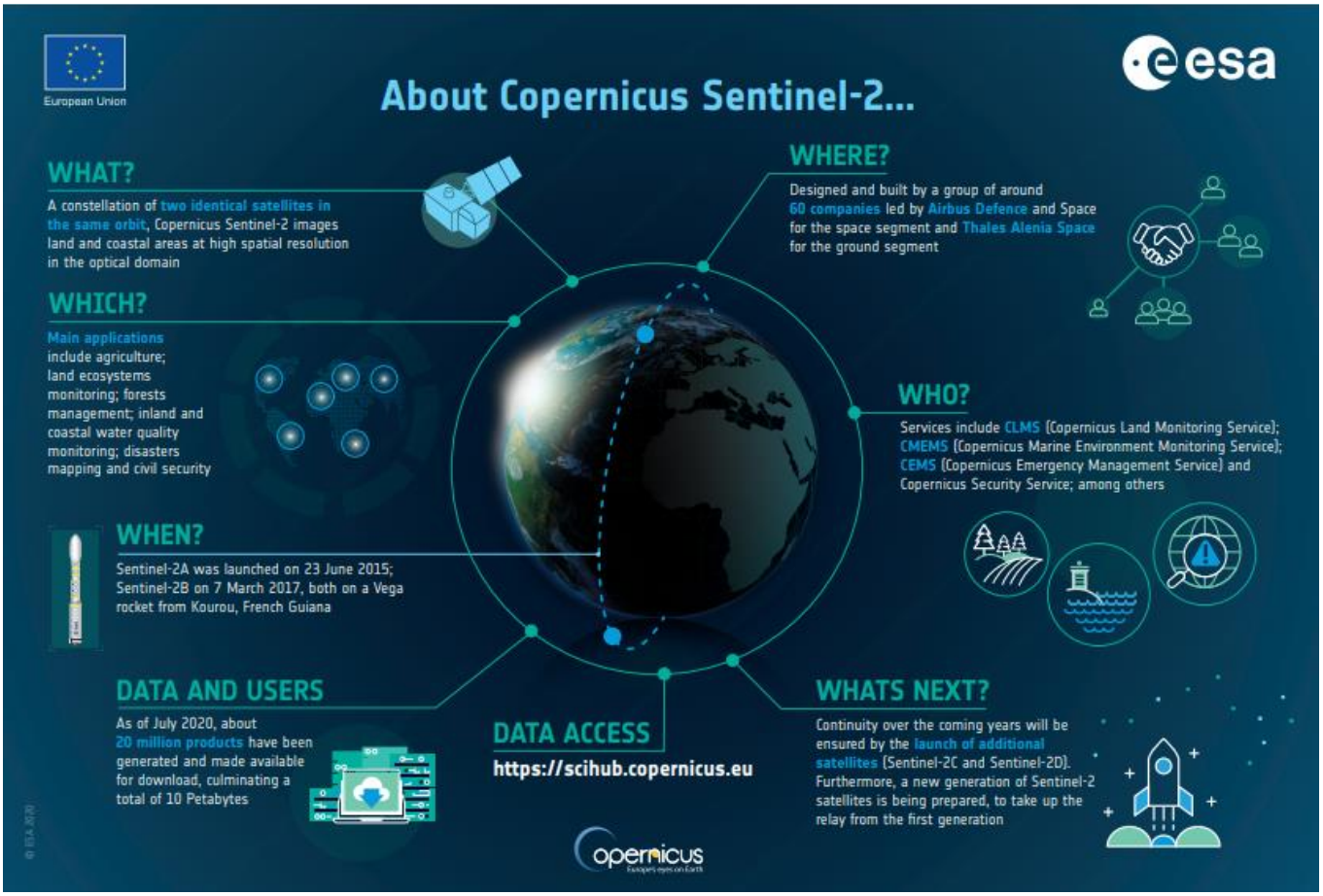

Figure 7:Sentinel-2 infographic (THE EUROPEAN SPACE AGENCY)

3.3. SYNTHETIC APERTURE RADAR (SAR) IMAGERY FOR FLOOD MAPPING

Synthetic Aperture Radar (SAR) sensors, are considerably different from optical data, being active sensors operate independently of the sunlight transmitting their own energy to illuminate the target and record the wave echoed back from each object. SAR works on microwave portion of the spectrum (see figure 4), with longer wavelengths, providing different information.

Microwaves offer a different perception of the Earth's surface compared to sensors operating in the visible and infrared parts of the spectrum due to their long wavelength, microwaves can penetrate clouds and sometimes even vegetation canopies to collect information about the terrain underneath forests. Then again, these instruments can gather information about many physical properties like the surface roughness and the moisture content for instance (Ulaby, F., Long, D., Blackwell, W., Elachi, C., Fung, A., Ruf, C., Sarabandi, K.,, 2014). Radars are one type of active microwave sensors.

The SAR is an imaging radar with microwave pulses transmitted by its own antenna, and receives the echoed energy reflected back from the target to the sensor, called the backscatter (Ozdemir, 2012). SAR was basically used by the military to carry out tasks related to tracking and gathering intelligence about the enemy. However, this technology started being studied in the last few decades by researchers, and it found an assembly of applications spanning from archaeology, precision farming, detection and monitoring of sea ice, disaster management and assessment of damages caused by floods (Ozdemir, 2012). SAR also captures the phase information which evidenced useful in interferometric techniques to measure the ground deformations caused by earthquakes (Lee, W. J., Lu, Z., Jung, H. S., and Ji, L. , 2017) and landslides (Raspini, F., Ciampalini, A., Del Conte, S., Lombardi, L., Nocentini, M., Gigli, G.,, 2015)

SAR sensors are shown in figure8 with the corresponding wavelengths. The frequency of the SAR sensor determines the remote sensing application and the kind of information that can be extracted from its products (Campbell, J. B. and Wynne, R. H., 2011)

Band	Wavelength
P-band	77 - 107 cm
L-band	15 - 30 cm
S-band	7.5 - 15 cm
C-band	3.75 - 7.5 cm
X-band	2.40 - 3.75 cm

Figure 8: Commonly-used SAR frequency bands and their wavelengths (Campbell and Wynne, 2011)

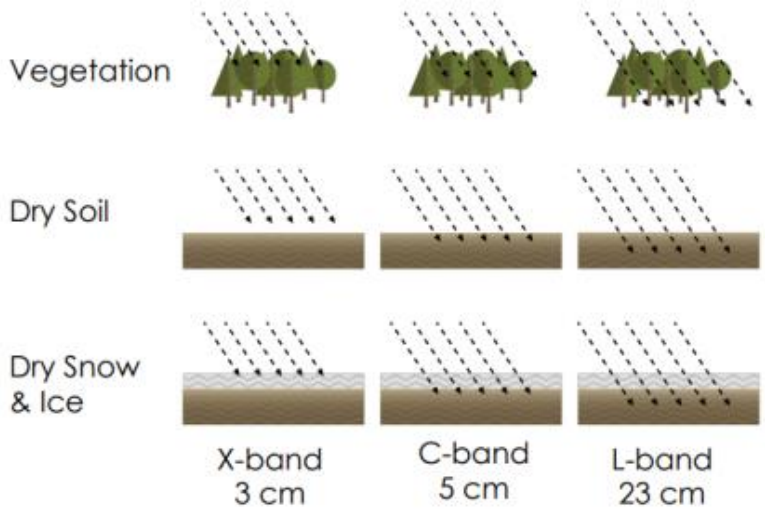

Figure 9: Penetration depths of X-band, C-band and L-band frequencies in a vegetation canopy, a dry soil, and a dry snow and ice (Podest, 2017)

Figure 9 illustrates how radar beam has varying degrees of penetration according to its wavelength., the same area is perceived differently by a short-wavelength sensor compared to a long-wavelength one. In the end, C-band sensors, due to their medium wavelength, reach a good compromise between flood mapping and canopy penetration. Due to the help of multi-frequency data, the flood extent could be delineated more precisely by avoiding difficulties to interpret complex backscatter variations in certain types of land cover (Boni, G., Pierdicca, N., Pulvirenti, L., Squicciarino, G., and Candela, L., 2015)

Seasat, launched in 1978 by the National Aeronautics and Space Administration (NASA), was the first satellite used for civilian applications to carry onboard a SAR sensor. This mission had as an objective to monitor the ocean, but it was unfortunately short-lived due to a technical failure on the same year it was launched (Ozdemir, 2012). After this mission, many other SAR sensors from other countries were launched including ESA's ERS-1 and ERS-2 missions in 1991 and 1995 respectively, which contained radar sensors in their payloads. The short wavelength X-band sensor carried aboard TerraSAR-X and CosmoSkyMed provides the finest resolution in the market up to now. TerraSAR-X is a commercial X-band SAR satellite launched in 2007 to meet the requirements of both the scientific community and the defence industry. In 2010, TerraSAR-X was joined in orbit by its twin satellite TanDEM-X. The Canadian Radarsat-2, launched by the end of 2007, operates in the medium wavelength C-band frequency and manages to achieve a metric resolution. The first British satellite SAR sensor is the low-cost NovaSAR-1 delivered into orbit in September 2018, and is primarily targeted at maritime observation. NovaSAR-1 operates in the S-band to reach a 6 m-resolution for a swath of 15 to 20 km (Cohen, M., Larkins, A., Semedo, P. L., and Burbidge, G., 2017). The SAR sensor with the longest wavelength is the Japanese L-band PALSAR-2 launched in 2014. The radar energy from PALSAR-2 is theoretically capable of penetrating forest canopies thanks to its wavelength. Sentinel-1 is different from the SAR commercial satellites just mentioned in that its products are available free of any charge, and it acquires images systematically without being tasked, except after being requested in emergency situations. Moreover, the revisit time offered by the constellation of Sentinel-1A and Sentinel-1B is of 6 days only.

3.3.1. Sentinel-1

Sentinel 1 is the European Radar Observatory for the Copernicus joint initiative of the European Commission (EC) and the European Space Agency (ESA). Sentinel-1 mission is designed as a two-satellite constellation and provides with continuous all-weather, day-and-night imagery at C-band Sentinel 1 comes in 2 levels, Sentinel-1 Level 1 (L1) and Level 2 (L2) products. Sentinel-1 has been designed to address primarily medium- to high-resolution applications such as monitoring sea-ice zones and the polar environment; mapping in support of humanitarian aid in crisis situations; surveillance of marine environments; monitoring land surface motion risks; and mapping of land surfaces, forest, water and soil, agriculture. Emergency operations shall be completed typically within 24 h, and in no case more than 48h after a user request has been issued. More Sentinel 1 specifications are summarized in Table 2. (THE EUROPEAN SPACE AGENCY)

Sentinel 1 Specification	
Satellite Lifetime	7 years
Products	L1 and L2
Constellations	2 satellites, Sentinel-1A and Sentinel-1B
Coverage	up to 400 km
Distribution	Raw, SLC, GRD, OCN
Mode	Strip Map mode (SM), Interferometric Wide-swath mode (IW), Wave mode (WV) and Extra Wide-swath mode (EW), depending on which the polarization, resolution, incidence angle, phase error, swath, radiometric accuracy are affected.
Processing level	Level 0, 1, 2
Revisit Time	12 days in a single pass, 6days two-satellite
Launched	03 April 2014 - Sentinel-1A 25 April 2016 - Sentinel-1B
Site	Kourou, French Guiana
Rocket	Soyuz rocket
Radiometric accuracy	for all measurement modes to be within 1 dB (3σ) and 0.5 dB (3σ)
Price	Free of Charge upon user registration
Polarization	Like polarized HH, VV Otherwise Cross polarized HV, VH

Table 2: Sentinel-1 Specification Summary (THE EUROPEAN SPACE AGENCY)

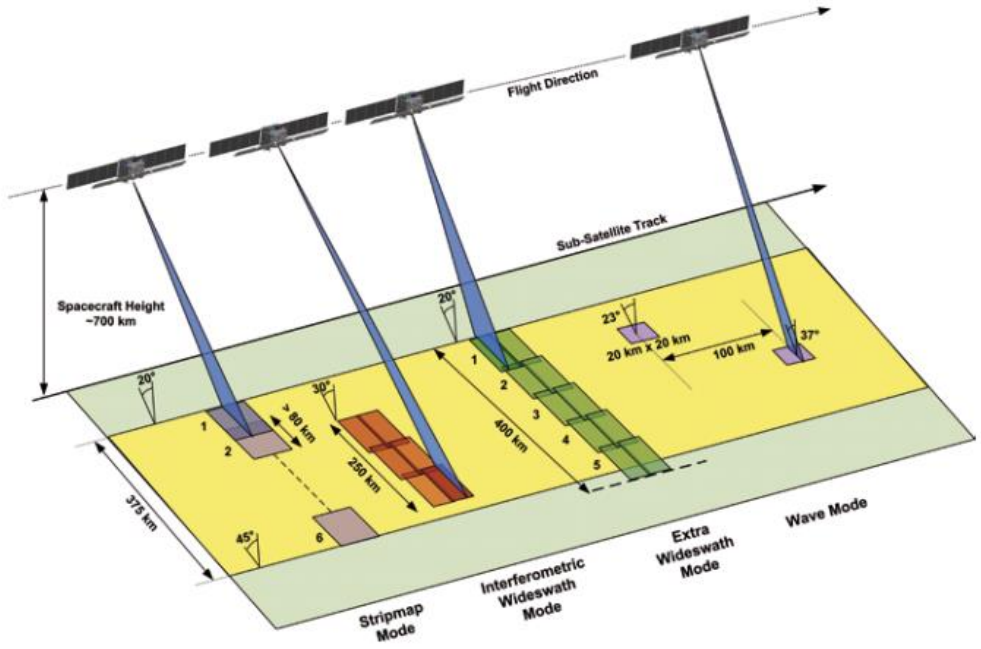

Figure 10: Sentinel 1 Modes

Sentinel-1 data products are distributed by European Space Agency (ESA) and include:

- Raw Level-0 data (for specific usage)
- Processed Level-1 Single Look Complex (SLC) data comprising complex imagery with amplitude and phase (systematic distribution limited to specific relevant areas)
- Ground Range Detected (GRD) Level-1 data with multi-looked intensity only (systematically distributed)
- Level-2 Ocean (OCN) data for retrieved geophysical parameters of the ocean (systematically distributed).

3.4. SAR AND OPTICAL IMAGERY DATA FUSION FOR MAPPING AND MONITORING

Data fusion involves the "combination of two or more different images to form a new image by using a certain algorithm" (Pohl, C., & Van Genderen, J.L., 1998).

Fusing different Remote Sensing scenes can enhance cartographic object extraction, and improve spatial resolution (Ehlers, 1991; Mangolini, 1994). Hence, there is an increasing interest in data fusion of multisource Remote Sensing acquisitions (Amarsaikhan, D., & Douglas, T., 2004); (Byun, Y., Han, Y., & Chae, T., 2015) . Over time, the availability of earth observation data has improved and it now covers different portions of the electromagnetic spectrum at different spatial, temporal and spectral resolutions (Pohl, C., & Van Genderen, J.L., 1998). This provides users with multiple data choices, but also creates additional challenges related to preserving the original spectral characteristics of the input image data (Ehlers, 2004) in the resulting fused images.

Multisensory data consisting of SAR and multispectral imagery positively impact the accuracies in various applications as well as reduces the disadvantage of working with the different types of data separately.

Optical imagery has high potential for rapid disaster mapping since it is available from a multitude of sensors and relatively easy to interpret due to its band composite in the visible wavelength range. Nonetheless, using optical data has a series of drawbacks when used for flood mapping (Sunuprapto, H., & Hussin, Y. A., 2000), (Estel, 2015). These include:

- Affected by daylight and weather conditions e.g., clouds, shadow.
- Neither penetrates vegetation nor soil, only detects surface tops.
- Not responsive to dielectric properties.
- Affected by topographical effects.
- Affected by sun-glint

On the other hand, SAR data also has a variety of limitations to be considered in the process of data selection:

- Often limited to binary segmentation into flooded and non-flooded.
- Inaccuracy in recording floods in urban areas (corner reflection principle).
- Noise and increased measurement uncertainty due to speckle.
- Higher difficulty to interpret information
- Geometric distortion

Therefore, fusing the SAR and Optical Imagery in a way to complement each other could lead to better results for Flood monitoring. This is done after pre-processing on the different data separately to remove disadvantages that could affect the quality of the results. Figure 11 below describes the process necessary to fuse optical and SAR data.

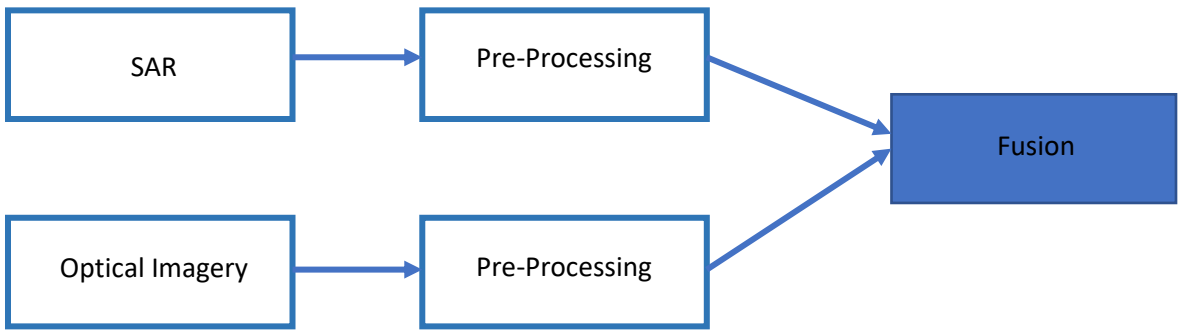

Figure 11: Steps to Image Fusion

4. DATA & STUDY AREA

The previous chapter introduced Remote sensing and Data used in remote sensing optical and SAR, commercial and free data. It also presented particularly Sentinel 1 and Sentinel 2 that was used in this thesis for flood mapping and monitoring. This chapter will provide information about the datasets used to answer the research questions outlined in Chapter 1 of this thesis, and also describes the chosen Areas of Interest (AOI). Figure 20 shows the workflow followed to find suitable study cases to implement the methodology on and achieve the aim of the thesis presented.

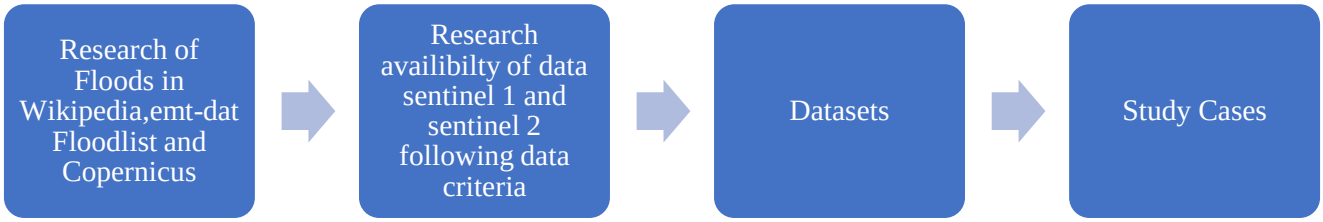

Figure 12:Workflow of Finding Suitable Case Study

4.1. RESEARCH STUDY CASES

4.1.1. Detecting a Potential Flood

Step one of the thesis was to find suitable events with accessible and available satellite images acquired both with SAR and optical sensors. The available databases have been explored (Copernicus, floodlist.com, disastercharter.org, emdat.be, Wikipedia etc.) to find information about floods which occurred between 2015 - present. The Sentinel satellites imagery has been selected, due to their characteristics and to their availability free of charge. Since the Sentinel-1 satellite started collecting data in April 2014 and Sentinel 2 in June 2015, the possible range of research starts from 2015 until the present. However, an important factor to consider was the location. To qualify some event as a potential for further research, it has to have enough additional information other than the satellite imagery. That can be problematic because, to some extent, the quality of data like road network or other shapefile as secondary data were not always available for all regions. This process required a considerable effort.

4.1.2. Detecting Availability of Data

This step consists of two simultaneous searches for Sentinel-1 image and Sentinel-2. Both searches should result in images that follow criteria mentioned in the section 3.1.2.1 Data Criteria. The Dataset used for both case studies are the ones with the least cloud coverage. Section 3.2 depicts the Dataset used. The choice of the most efficient method for water identification and mapping depends on the type of satellite information (optical or radar) as well as on the spatial resolution this information could provide (Jiri Marsalek, 2006).

4.1.2.1. Data Criteria

Chosen data had to follow certain selection criteria to obtain the best results in flood delineation. The Sentinel 1 and Sentinel 2 dates should not be very different from each other, so that the extent of the flood has not changed over time, as well as, being in the time range of the flood event occurrence. The percentage of clouds shouldn't be more than 40%. The Sentinel 1 and Sentinel 2 should be overlapping and covering the complete AOI.

4.2. DATASETS

Data products from Sentinel-1 and Sentinel-2 are freely available on the Copernicus Open Access Hub (https://scihub.copernicus.eu/). Registered users can choose the place, date, data type and other required parameters and download the data. However, download speeds are limited to two datasets at a time per user. Due to flooding that is always coupled with thick clouds layer a lot of Sentinel 2 scenes were available but with almost 98 – 99 % of cloud coverage. Dataset for Spain Zaragoza and France Nice were used for this thesis presented in the next section. The Dataset used for both case studies are ones with the least cloud coverage.

4.3. SPAIN - EBRO RIVER CASE STUDY

The Ebro river, Figure12, runs through seven autonomous communities and its hydrographic basin is one of the largest in the Iberian Peninsula. Its average contribution, of about 14 km^3 per year, represents almost 4% of the total Mediterranean basin contributions. The Middle Ebro River presents a meandering channel with a very low slope. The average width of the floodplain is 3.2 km, having a maximum width of 6 km. Its great extent favours geological, topographic, climatic, and water balance variability. In the Middle Ebro River stands out the remarkable increase of discharge contributed from the Aragon River basin, which drains the Western Pyrenees. Thus, flooding processes are common in this river reach, but the combination among decrease of discharges, dam construction and expansion and reinforcement of defences have created an unusually quiet period as regards flooding events during the last quarter of the previous century. Nevertheless, with the turn of the century, it seems that the Middle Ebro River has entered into new dynamics, with bigger and more frequent flooding. Important flooding episodes appear around the city of Zaragoza in spring, given when snow melts in the Pyrenees or due to the excessive precipitation and surface runoff, being them the cause of extensive damage, loss of property and human suffering (S. Domenech, 2009).

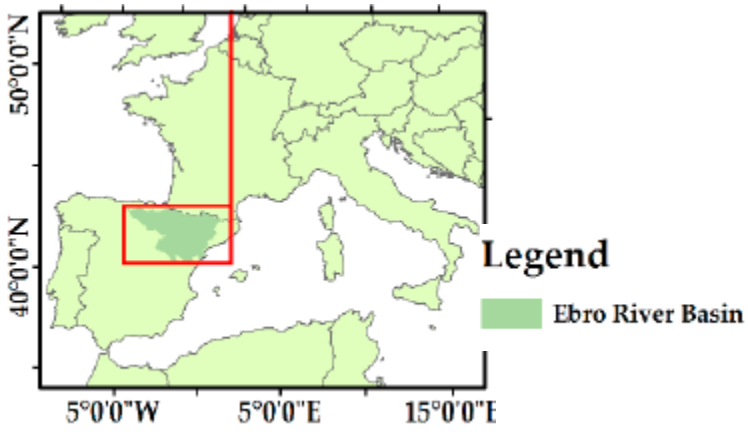

Figure 13: Ebro River in Spain (S. Domenech, 2009)

The study area is focused in Zaragoza province which has an area of 973.78 square kilometres and coordinates of 41° 38' 58.8948" N and 0° 53' 15.7632" W. Figure 13, highlighted with a darker box and red circle. The Ebro at Zaragoza stood at 4.86 metres, above the alert stage of 4.5 metres, with flow rates of 1,785 m3/s (Flood List, 2018).

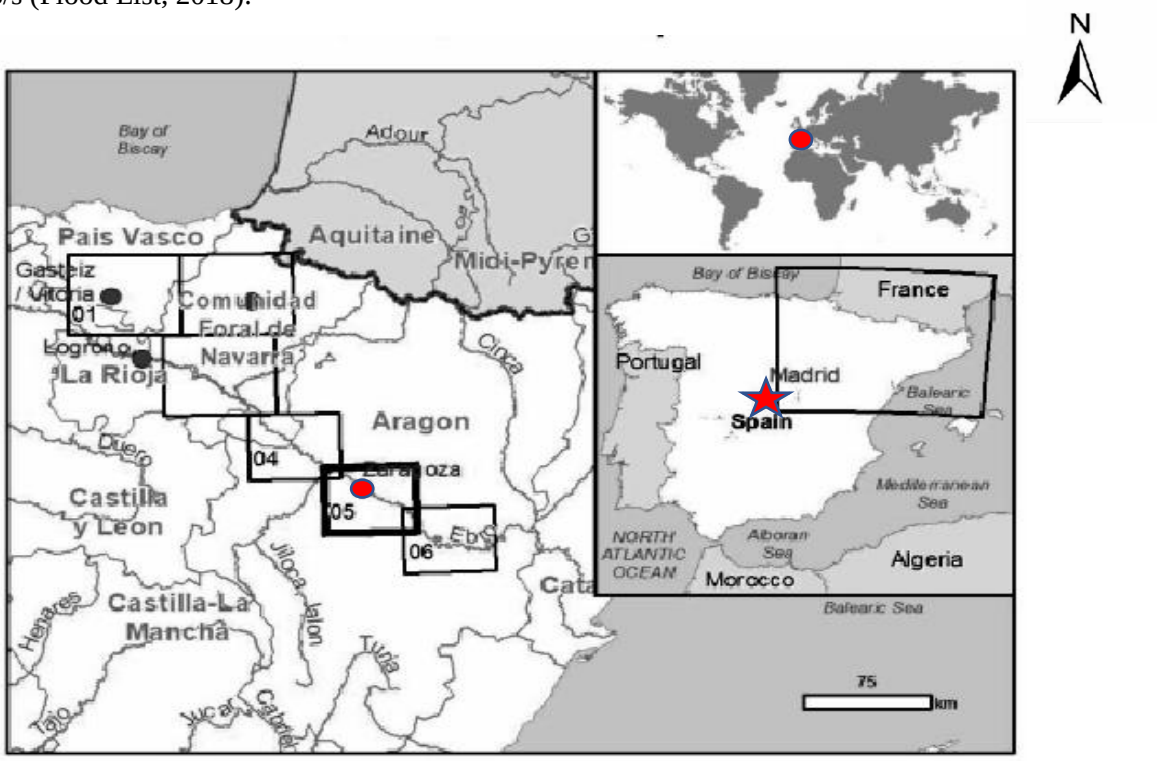

Figure 14: Ebro River and AOI - Zaragoza

Various high-water events of different magnitudes have been observed in the Middle Ebro, in 12th April 2018, an extraordinary flood event occurred in the Ebro basin due to the snow that melted in the Pyrenees. The firsts flooded areas were registered in Caste Jón (Navarra) and the peak in Zaragoza city foreseen on 15th April around 12:00 UTC. Blocking of an entire neighbourhood in Zaragoza and shut the provincial highway.

Event	Navarre and Aragon Regions, North East Spain, April 2018
Date	April 12 to April 16, 2018
Type	River flood
Cause	Extreme rainfall, Snow melt
River level	4.86 m
Alert stage	4.5 m
Fatality	1

Table 3:Flood Event Details (Flood List, 2018)

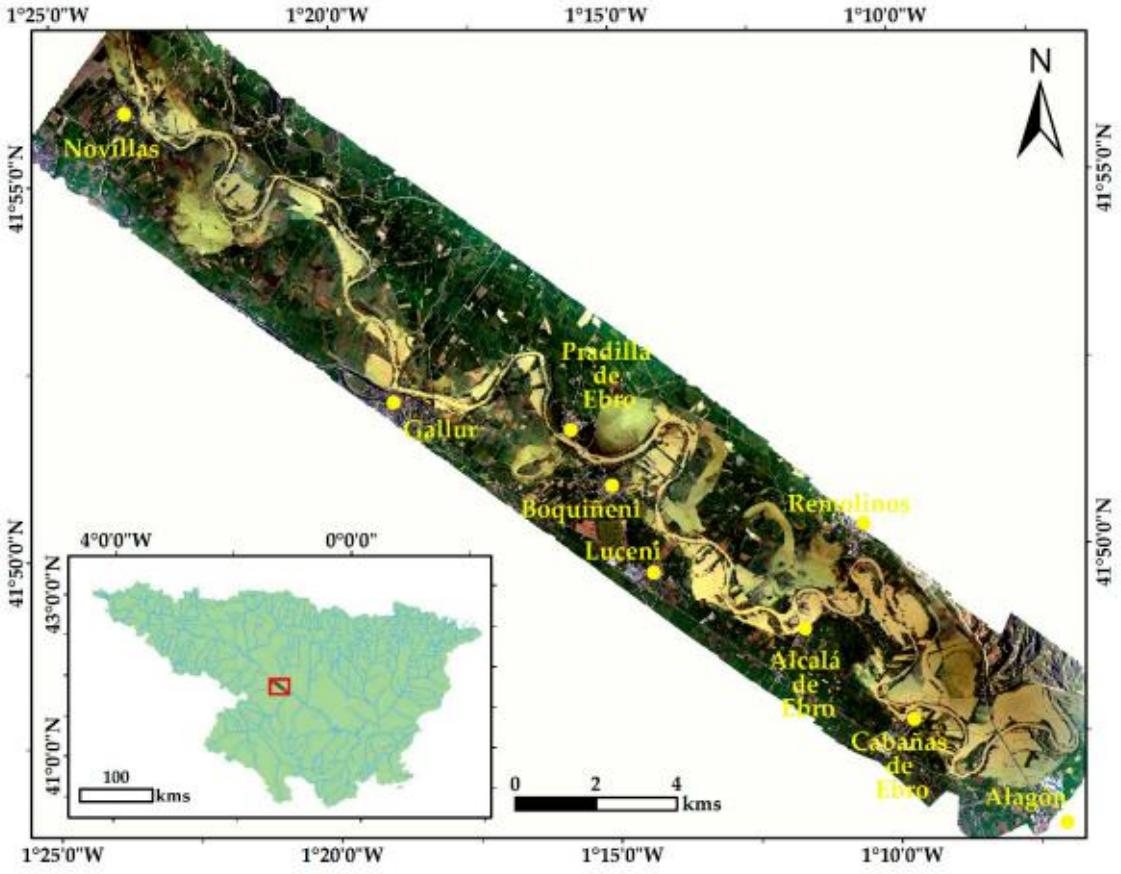

Figure 15:Ribera Alta orthophotography on 14 April 2018 (Confederación Hidrográfica del Ebro, CHE, 2018)

This favours a greater understanding of the water behaviour of the Ebro river over time. For the study area, a vertical aerial photograph corresponding to a part of the section that the CHE called "Ribera Alta" was used (Figure 15), captured on 14 April 2018.

The reason of the flood as specified above is the melting of snow that showed a huge increase from 2017 – 2018 then in 2016- 2017 as shown in figure 15.

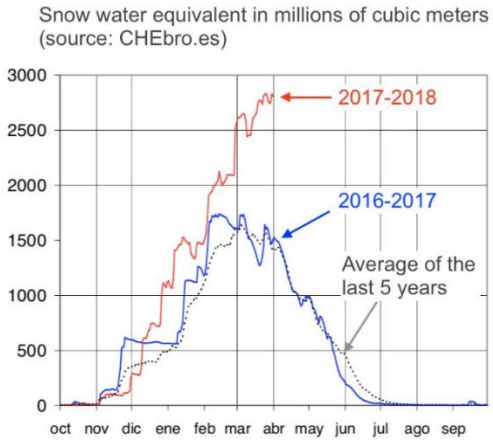

Figure 16:Snow melting comparison with an increase in 2017-2018 (CONFEDERACIÓN HIDROGRÁFICA DEL EBRO COMISARIA DE AGUAS, 2018)

Figure 16 below show some images that depicts how the flood event in April 2018 affected Ebro river area.

Figure 17:Flood Damage (Flood List, 2018)

4.4. DATASET FOR SPAIN – ZARAGOZA

Sentinel 1 and Sentinel 2 data were used to understand how fusing these two sources of data would result in higher accuracy in flood monitoring, specified below are some of the basic Specification of these Datasets used in Zaragoza case study.

Sentinel 2			
Data	Date	Cloud Coverage	Projection
S2A_MSIL2A_20180414T105651_N0207_R094_T30TXL_20180414T112338	14/04/2018	31.4%	UTM WGS Zone 30N
S2A_MSIL2A_20180414T105651_N0207_R094_T30TXM_20180414T112338	14/04/2018	31.4%	UTM WGS Zone 30N
Sentinel 1			
Data	Date	Projection	
S1A_IW_GRDH_1SDV_20180413T175451_20180413T175516_021452_024F10_6834	13/04/2018	UTM WGS Zone 30N	

Table 4: Zaragoza Dataset

4.5. FRANCE ALPES-MARITIMES CASE STUDY

France experiences catastrophic floods on a yearly basis, with significant societal impacts. A potential 2°C increase in global temperatures would likely further intensify this problem by significantly increasing flood probability (Roudier P, 2016) and severity.

NatCatSERVICE report (NatCatSERVICE, 2017) which is provided by Munich Re to the European Environment Agency under institutional agreement, and which illustrates the impacts of extreme weather and climate related events in the European Economic Area (EEA) member countries (1980-2017), ranks France as having had the most flood-related fatalities (from extreme weather and climate related events) in Europe (approximately 23,500 over the 1980-2017 period). Furthermore, according to (Paprotny D, 2018), while overall exposure to floods has declined in most European countries, mostly in central and northern Europe, relative exposure has increased in France and other western states (i.e., Germany, Netherlands) seemingly because of intense urbanization processes, occupying and transforming flood prone land.

On 2nd to 3rd October 2020 red warnings were issued by National central forecasting centre (meteorological and hydrological) for France, areas of Alpes-Maritimes Department (Figure 17), which were among the hardest hit by Alex Storm leading to heavy rainfall and extensive flooding. Hundreds of homes are thought to have been destroyed and several damages occurred to infrastructures and buildings. "We have actually had houses wiped out," said Alpes-Maritimes prefect Bernard Gonzalez. for the night between 02/10 and 03/10.

Figure 18: Alpes Maritime highlighted in France Map

Particularly speaking, Alex storm, ravaged several villages around the city of Nice on the French Riviera. Nice Mayor Christian Estrosi called it the worst flooding disaster in the area for more than a century after flying over the worst-hit area by helicopter. (CNN, 2020). The city of Nice is a big French city located south east of France, located in the department of Alpes-Maritimes of the region Provence-Alpes-Côte d'Azur. The latitude and longitude of Nice are 43.706 degrees North and 7.262 degrees East.

Area:	**71.92 km² (7 192 hectares)**
Maximum altitude:	520 m
Average altitude:	260 m
Altitude of the city hall:	10 m

Table 5:Specification of Nice City (Map-France.com)

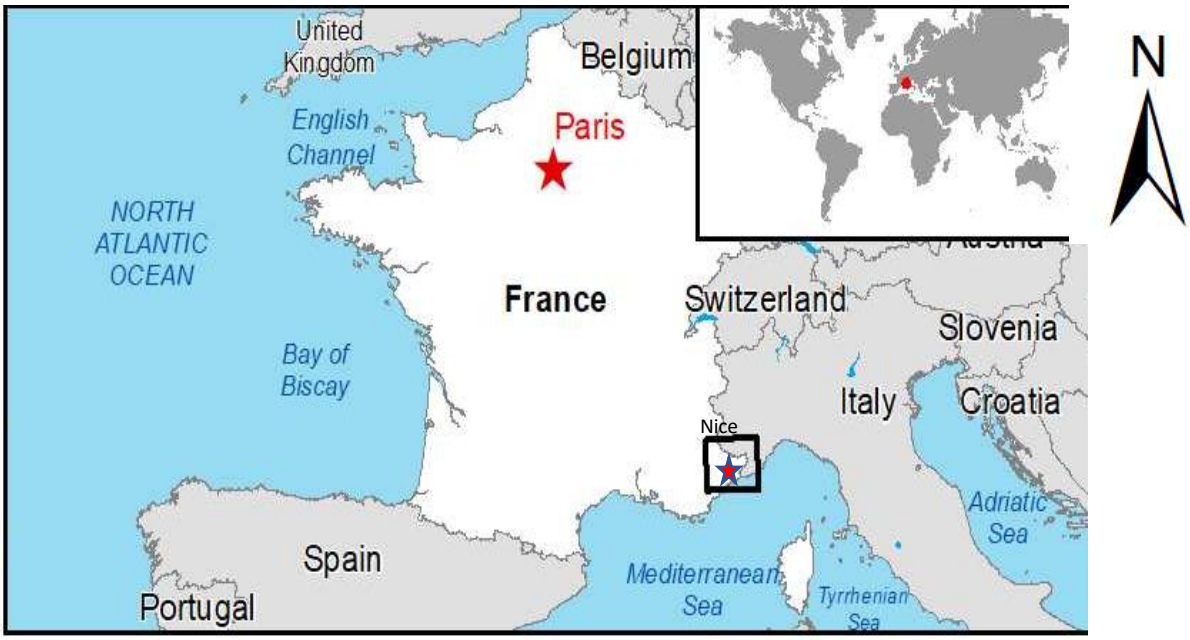

Figure 19:Nice-France (European Commission, Joint Research Centre, 2020)

The disaster on 2nd and 3rd of October 2020 not only caused flooding but massive landslides, destruction to properties and a number of fatalities as mentioned in table 6 and in Figure 19.

Event	Floods in south eastern France and northern Italy
Date	October 2 to October 3, 2020
Cause	Alex Storm
Coupled Disaster	Landslide and Flood
Fatality	12

Table 6: Damage in Nice (European Commission, Joint Research Centre, 2020)

Figure 20: Landslide and Flooding due to Alex Storm (BBC)

4.5.1. Dataset for France – Nice

Sentinel 1 and Sentinel 2 data were also used for Nice (France) to understand how fusing these two sources of data would result in higher accuracy in flood monitoring, specified below are some of the basic Specification of these Datasets used in Nice case study shown in Table 7.

Sentinel 2			
Data	Date	Cloud Coverage	Projection
S2B_MSIL1C_20201003T101759_N0209_R065_T32TLP_20201003T141329	03/10/2020	7.4%	UTM WGS Zone 32N
Sentinel 1			
Data	Date	Projection	
S1A_IW_GRDH_1SDV_20201003T172246_20201003T172311_034635_040884_80B9	03/10/2020	UTM WGS Zone 32N	

Table 7: France Nice Dataset

5. METHODOLOGY

The previous chapter has described the data sources and data criteria which were used in this study and has presented the chosen test areas that are used to map the flood extent using remote sensing through data fusion. The focus of this chapter is on the methods used. This chapter will start with definitions of the pre-processing workflow required before any quantitative analysis on Remote Sensing images (Sentinel 1 and Sentinel 2). The workflow shown in figure 21 underlines the methodology main divisions explained in this thesis Pre-Processing of Sentinel 1 and Sentinel 2, Processing starting from data fusion of SAR and optical reaching to Flood Inundation which is the aim of this thesis and finally Accuracy assessment to evaluate the performance of the suggested method. The proposed method depend will be explained in detail in this Chapter. The Tool used for visualization, pre-processing and processing is the free software SNAP (Sentinel Application Platform) Tool version 8.0.0, created specifically by ESA for the analysis of the data captured by Sentinel satellites. The maps are produced using ArcGIS software.

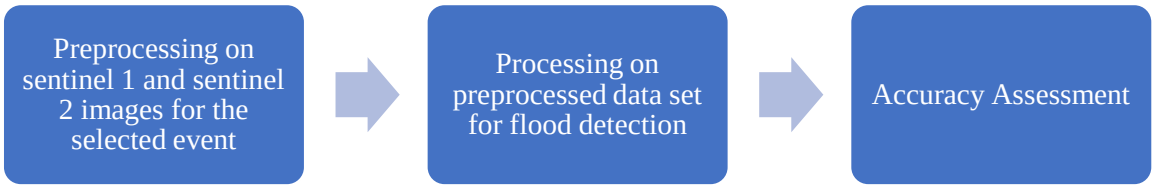

Figure 21: Workflow of Flood Delineation done on the AOI

5.1. FLOOD DELINEATION

One of the biggest problems is obtaining a clear picture of the overall extent of the flood. In the aftermath, risk maps can be created that combine a trio of variables – the flood extent, the type of land inundated and the likely flood return period – to guide civil protection officials as well as insurers as to how much money should reasonably be spent to protect or insure areas on the map from future floods (ESA). Flood Monitoring can be done using different techniques that differ in the required data, processing, time cost, and accuracy. Methods vary from hydrological methods, change detection, Classification (supervised classification, unsupervised classification and object-based classification) and visual interpretation etc. This thesis covers supervised classification that is to be explained in details in Flood classification section 5.4.2. This section starts with a very brief definitions of the pre-processing workflow for Sentinel 1 (calibration, terrain-correction, speckle-filtering, and co-registration) required before any quantitative analysis of SAR images and following pre-processing of Sentinel 2.

5.2. SENTINEL -1 PRE-PROCESSING

As shown in the previous figure 21 Pre-processing is the first step of the methodology that is done on Sentinel 1 and Sentinel 2, however, the pre- processing is not typical for both data types. Pre-processing of datasets step is necessary for the processing phase to avoid unnecessary noises thus removing errors and making the various data consistent during the processing that will affect the quality of the final output. For Sentinel 1 figure 22 states the sequence followed for the pre-treatment of the Sentinel 1 which follow a standard pre-processing chain for SAR. Each pre-processing step will be explained extensively in what follows.

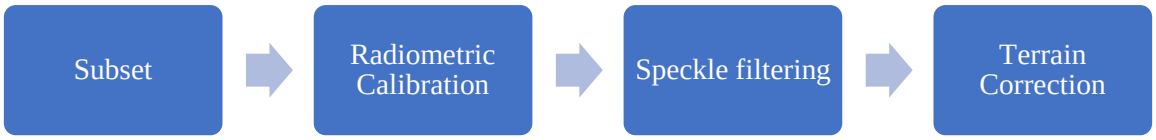

Figure 22: Pre- Processing Workflow

5.2.1. Subset

A subset is a section of a larger downloaded image. Since satellite data downloads usually cover more area than you are interested in you can select a portion of the larger image to work with (2021).Creating a Subset is based in our area of interest). it is to be used as an input for the next step so that only the subset area is radiometrically calibrated saving processing cost.

5.2.2. Radiometric Calibration

Performing Radiometric Calibration, the value representing the radar backscatter intensity; in units of decibels dB because of the wide range of values it can assume; is taken for each pixel. The backscattering coefficient σ_0 is the quantity obtained at each pixel after calibration of the distributed SAR image, is taken for each pixel, and σ_0 (The dimensionless backscattering coefficient)-bands are generated for the two polarizations that we provide, VH and VV (Tavus, et al., 2018; Ban, et al., 2017). There is the possibility of obtaining other bands, but the _0-band is the one that provides the best separation between terrestrial soil areas and those with water (Bioresita, et al., 2018).

Permanent water bodies have temporal heterogeneity regarding backscattering (Martinis, et al., 2015). The backscatter intensity values are usually below -20 dB and manifest themselves in dark, practically black tones. Applying the theoretical knowledge characteristic of the flat areas, the wave beams emitted by the sensor are reflected on the surface, which acts as a mirror, causing almost no return of energy towards the sensor; hence, its intensity value and representation in the radar image. There are surfaces that, at the scale of the measuring wavelength, behave as smooth and share almost identical scattering properties with water surfaces that can create “false positives” (Henry, et al., 2006).

5.2.3. Speckle Filtering

The speckle noise impedes the interpretation and cause degradation in the quality of SAR images. That is why, any classification of the SAR image is preceded by a speckle filtering, which tries to smooth out and reduce the noise while preserving the texture and edge information (de Leeuw, 2009). Mainly, noise is due to random oscillations of the signal returned to the sensor due to the interaction of the emitted wave with

the rough terrain surfaces (Senthilnath, et al., 2013). Many methods for speckle reduction exist in the literature. The speckle present on SAR images is assumed to be a multiplicative noise, since it grows proportionally to the signal. This phenomenon can be easily confirmed in high-backscatter areas which appear grainier than darker ones. Adaptive filters like Lee filter, Frost filter, and the Gamma MAP filter build on this assumption, and are based on the local statistics of the image calculated within a moving window (Qiu, 2004).

5.2.4. Terrain Correction

SAR images suffer inherently from geometric distortions (layover and foreshortening) typical of side-looking radar images of elevated areas. A correction taking into account a digital terrain model and orthorectification allow to reduce distortions due to changes in the topography and the angle of incidence with the ground with respect to the nadir. Terrain correction used in this study was range doppler terrain correction and the digital elevation model (DEM)–SRTM-3Sec. This pre-processing operation is essential when the SAR dataset is used in combination with an optical one.

5.3. SENTINEL -2 PRE-PROCESSING

The above section described the pre-processing steps for Sentinel 1, similarly, Sentinel 2 data requires pre-treatment to reach to the required quality of input data for the fusion process of Sentinel 1 and Sentinel 2. These steps of pre-processing of both Sentinel 1 and Sentinel 2 are followed to ensure a trusted outcome limiting the uncertainties of the research objectives aiming at flood monitoring. The workflow in (Figure23) depicts the steps undergone for pre-treatment of Sentinel 2.

Figure 23:Sentinel 2 Pre-processing workflow

5.3.1. Resampling

Resampling is the technique of manipulating a digital image and transforming it into another form. This manipulation could be done for various reasons: change of resolution, change of orientation, i.e., rotation, change of sampling points, etc. This technique is used extensively in image processing for all applications, including medical, industrial and of course in remote sensing. This is because the image as it is captured will have limitations imposed by the imaging geometry or camera. However, for analysis, we would like to have the image in a different and better form. (Padmanabhan, 2005).

Creating multi-resolution product is currently not supported in SNAP. Therefore, it will not work to combine the different resolutions in one product. For fusing Sentinel 2 and Sentinel 1 it was needed to resample the multi resolution Sentinel 2. Sentinel 2 comes in bands with resolutions of the 10m, 20m bands and 60m, while Sentinel 1 comes with a resolution of 10m. Therefore, resampling was done to 10m for fusion. Resampling, is the first necessary operation, aimed to geometrically correct distorted pixels in the original imagery. Available resampling methods included: the nearest neighbour, bilinear interpolation, and

cubic convolution. The first option was chosen, as it allowed us to preserve the original pixel values. (David P. Roy, 2016).

5.3.2. Cloud Removal

Many studies have developed and tested different methods of cloud masking of Sentinel-2 images. For Sentinel 2 L1C, The Idepix Processor provides a pixel classification into properties such as clear/cloudy, land/water, snow, ice etc (Step Forum, 2017).The Idepix produces extra NDWI, water mask and other additional layers to separate features from each other easily.

5.3.3. Subset and Mosaicking (optional)

Lastly, both images were subsetted to the selected AOI this step is done for faster processing of data. Mosaicking is an optional step depending on whether the AOI is covered by a one or two Sentinel -2 image. After completing the required pre-processing steps the main processing on Sentinel 1 and Sentinel 2 is undertaken to reach the objective of flood monitoring.

5.4. PROCESSING ON PRE-PROCESSED DATA SET FOR FLOOD DETECTION

To Summarize, figure 24 shows the pre-processing steps undergone by Sentinel 1 and Sentinel 2 that were required for the start of processing that is the second step in the Workflow of Flood Delineation done on the AOI as shown previously in figure 21.

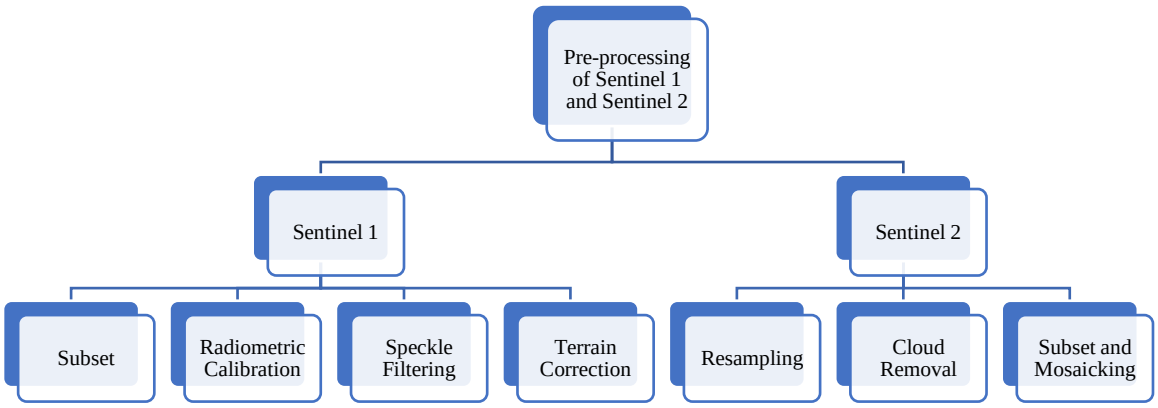

Figure 24: Complete Pre-Processing overview for Sentinel 1 and Sentinel 2

The processing starts with fusion of Sentinel 1 and Sentinel 2 reaching to extraction of landcover classes from the fused image using a training set and supervised classification method. These steps are necessary to achieve the aim of this thesis for flood delineation and detection and are explained in details in the following chapters.

5.4.1. Fusion of Sentinel 1 and Sentinel 2

This thesis aims at experimenting flood delineation by fusing multi sensor imagery after completing the pre-processing treatment on Sentinel 1 and Sentinel 2 separately as explained in figure 24 previously. The synergetic use of different information layers can help detect more precisely the areas affected by the flood, reducing false alarms, uncertainty and missed identifications which may affect algorithms based on data from a single source. Both the integration of multilevel information and the use of multi-sensor imagery increase the overall accuracy (Björn Waske, 2008). For an image segmentation or classification task, the goal of fusing data from different sensors is to reduce the classification error rate obtained by single source classification.
The input layers for data fusion employed in the model prediction stage include:

- Sentinel-1as a master layer
- Sentinel-2: All bands including NDWI, MNDWI layers as a slave layer.

The fusion was done through Collocate process in SNAP.

5.4.1.1. Collocation

The Collocation Tool allows to collocate (fuse) two spatially overlapping products, however they should have the same projection for both Sentinel 1 and Sentinel 2. The output product will contain all the bands from Sentinel 1 and Sentinel 2 data. Collocation requires 2 input products, one master product which determines the extent, pixel size and pixel registration of the output product, and one or more slave products which will be clipped and resampled accordingly. The Collocation module does not support multi-resolution products as master. Collocation works by iterating over all the pixels in the master products and tries to find the closest pixel in the slave product (Fabrizio_Ramoino, 2017).

The collocation for Sentinel 1 and Sentinel 2 was done using Sentinel 1 as master and s2 as slave mainly due to the fact that Sentinel 2 was had No Data value due the cloud masked regions as well as due the resampling that was done to Sentinel 2 bands. Trials were done of removing the 20m and 60m in the classification but the results were not as good as with all the layers. Therefore, the input for the fusion were as shown in the below table:

Master Product	Pre-Processed Sentinel 1 bands
Slave product	Pre-Processed Sentinel 2 bands along with the NDWI produced using Idepix for cloud removal
Other Inputs	Vector layers as training samples for the different classes

Table 8: Collocation Inputs

5.4.2. Flood Classification

Fusing the Sentinel 1 and Sentinel 2 as explained in the previous chapter is an important step that allows for the synergetic detection of flooded area in study cases. In the recent years, significant efforts have been devoted to the implementation of a monitoring methodology. From the operational point of view, during dangerous floods, and preference is given to simple and fast methods (Jiri Marsalek, 2006). Traditionally, different pattern recognition methods and machine learning algorithms have been used to automatically classify multi-temporal remotely sensed images and to extract change information. These typically rely on methods for identifying different categories associated to complex land surfaces. These methods include but are not limited to change detection and Classification both supervised and unsupervised. Change detection involves the analysis of at least two remote sensing images acquired over the same geographical area at different times. Whereas, classification is one of the major approaches to infer land cover information from remotely sensed data (Alberto Refice, 2017). The next section introduces the supervised classification and the methods of supervised classification that are implemented in this thesis.

5.4.2.1. Supervised Classification

Supervised classification is a common approach for information extraction from images and consists of two main stages: training and classification. During the training stage, a set of representative labelled samples are selected for each class which are pairs of input and expected output data. The derived model can be as simple as a function that maps the given input to the corresponding output in the training dataset. Once trained, a classifier is used for the assessment of the probability of every image pixel to belong to the classes. In a remote sensing application, the training samples are either collected on the ground using in situ surveys, or manually digitized by an expert from airborne or satellite data. Supervised learning algorithms have been adopted by various sectors recently such as the manufacturing and the financial industries. Other applications that make extensive use of supervised learning are virtual personal assistants, image recognition on social media, and autonomous cars.

5.4.2.2. Random Forest supervised classification

In this study, the RANDOM FOREST classification method implemented in the ESA SNAP Tool was applied for determining the flooded areas. The random forest algorithm, proposed by L. Breiman in 2001, has been extremely successful as a general-purpose classification and regression method (Gérard Biau, 2015). RF is a machine learning algorithm. It builds upon the concept of decision trees. Random forest builds multiple decision trees and merges them together to get a more accurate and stable prediction (Niklas Donges, 2020). A random forest is a predictor consisting of a collection of M (Number of trees in the forest) randomized regression trees. To classify a new object based on attributes, each tree gives a classification and we say the tree “votes” for that class. The forest chooses the classification having the most votes (over all the trees in the forest) and in case of regression, it takes the average of outputs by different trees (VIDHYA, 2016). The approach, which combines several randomized decision trees and aggregates their predictions by averaging, has shown excellent performance in settings where the number of variables is much larger than the number of observations (Niklas Donges, 2020).

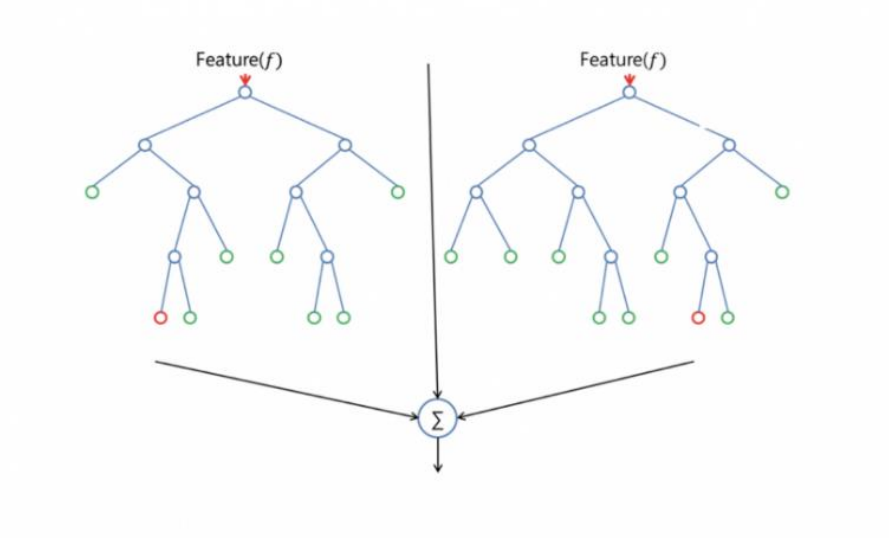

Figure 25: Random Forest Decision Tree

In this study, a land cover map with four classes including the flooded surfaces has been produced in SNAP software using the Random Forest method. Different combinations of feature sets were also tested in a selected sub-area. Four classes were determined (permanent and flooded water surfaces, urban, forest, agriculture). The training areas (polygons) for each class were delineated from the pre-processed Sentinel2 data, the water training sample were taken also using NDWI with visual interpretation and different bands of Sentinel 2 have been considered. The training areas were selected over colour combination that ensures maximum visibility of the required class from the Sentinel 2 image. As mentioned before, other Supervised classification methods were experimented with the highest accuracy found using Random Forest and following is KDKNN in SNAP.

5.4.2.3. KD KNN supervised classification

K-D tree: KD tree is a tree-based specific data structure for efficiently representing our data (SINGH, 2017),. The k-d tree is a data structure invented by Jon Bentley in 1975. Despite its fairly old age and there exist a number of spatial index structures in literature; however, k-d tree and its variants remain probably the most popular data structures used for searching in multidimensional spaces, at least in main memory. A k-d tree, or k-dimensional tree, is a data structure used for organizing some number of points in a space with k dimensions. It is a binary search tree with other constraints imposed on it. K-d trees are very useful for range and nearest neighbour searches. Typical algorithms construct k-d trees by partitioning point sets recursively along with different dimensions. Each node in the tree is defined by a plane through one of the dimensions that partitions the set of points into left/right (or up/down) sets, each with half the points of the parent node. These children are again partitioned into equal halves, using planes through a different dimension. Partitioning stops after log n levels, with each point in its own leaf cell. The partitioning loops through the different dimensions for the different levels of the tree, using the median point for the partition (Otair, 2013).

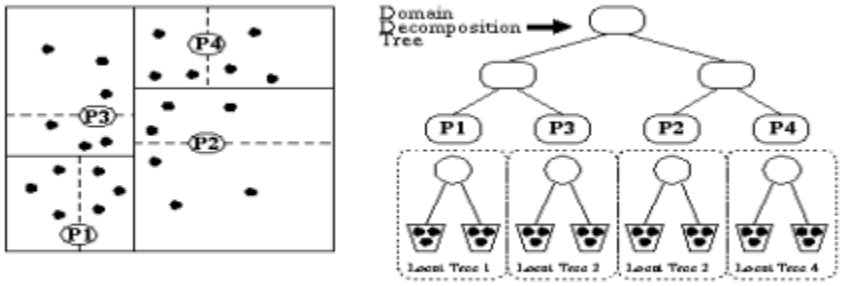

Figure 26: KD KNN Supervised classification Partitioning

The KD KNN Supervised classification was used in this thesis along with Random Forest supervised classification and comparison if each method was done along with the results highlighted in chapter 6 of this thesis.

5.5. ACCURACY ASSESSMENT

Finally reaching to the accuracy check that is required to conclude if the method followed in the previous chapters for flood delineation is useful and results in a more accurate output for the water extent or contradicts the assumption that fused data improves the result of accurate flood mapping. Reference maps were available to compute the accuracies of the derived flood maps. The water extent classified is assessed against Reference maps as well as the Collocated Sentinel 1 and Sentinel 2 images taken during the flooding. This to verify that the method of fusing the multisensory data will add up to the accuracy of classification thus complimenting each other. The accuracy scores allow to infer the agreement rate between the produced flood map and the corresponding reference, and to tell whether the flood is underestimated or overestimated. The Intercomparison was carried out by collecting Intercomparison point done using SNAP software from 30 – 80 per class were taken the advised range is between 30 – 50 per class. Figure 27 shows an example of test points taken on France Nice Fused image for performing Confusion Matrix for the Results obtained. Figure 28 shows Intercomparison point against Copernicus Reference Image for the same flood France Nice October 2020.

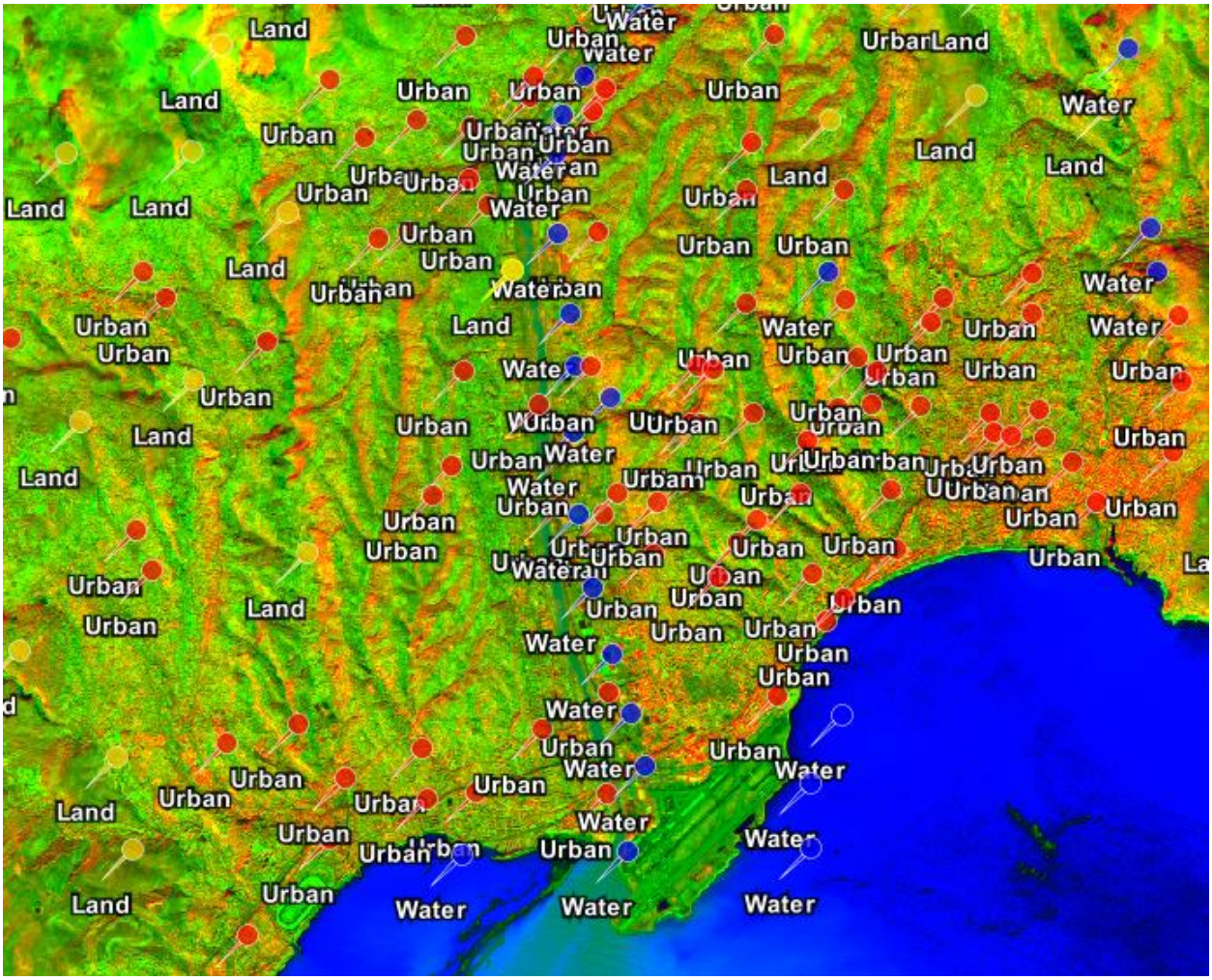

Figure 27: France-Nice Intercomparison Points in Fused Sentinel 1 and Sentinel 2 Image

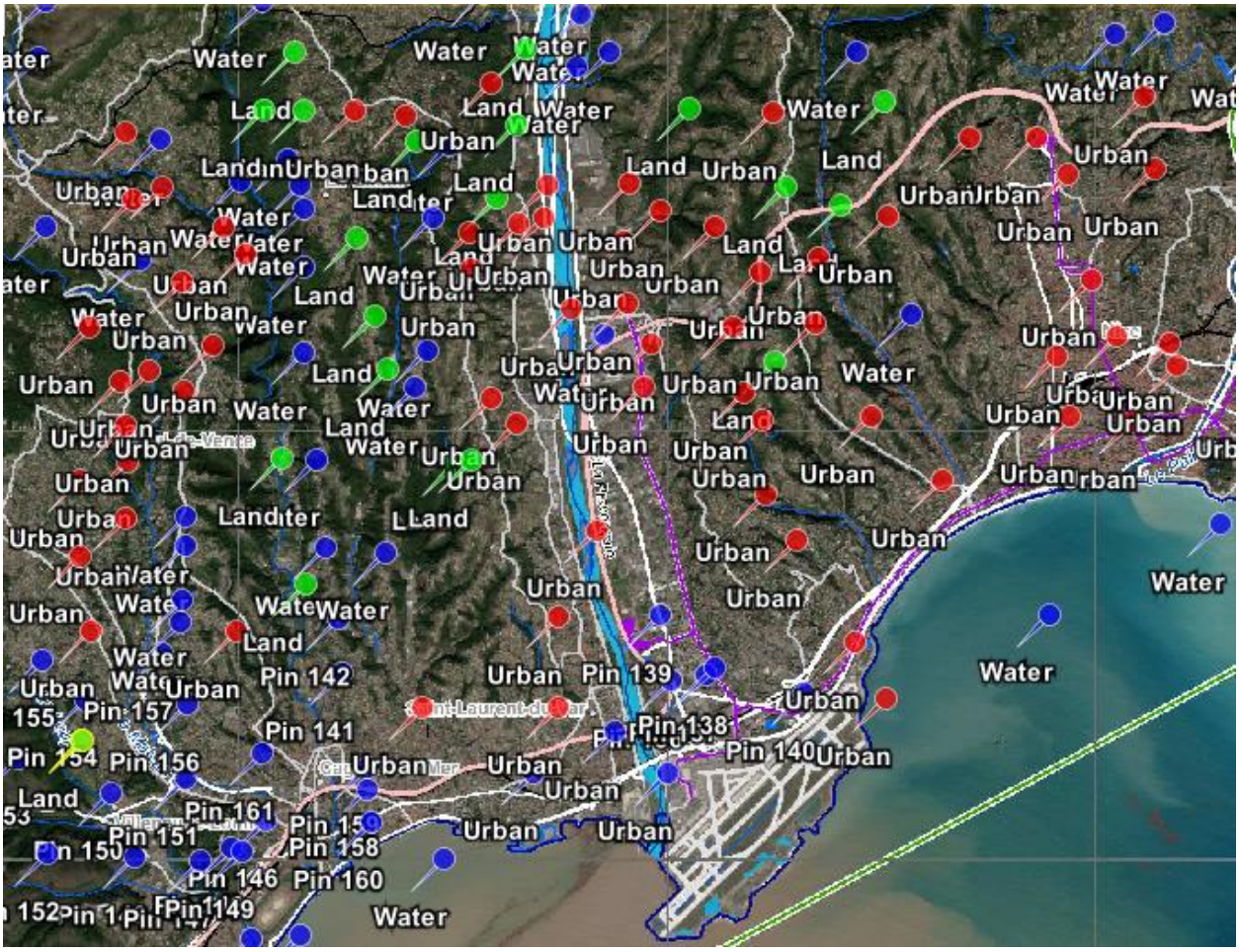

Figure 28: France-Nice Intercomparison Points in Reference Copernicus image

Confusion matrix shows a number of correct and incorrect predictions by comparing two data sources and therefore, is used to assess the accuracy of classified image by comparing the classification result with reference image and the fused image. Confusion matrix reports the overall accuracy, kappa coefficient, error of commission and error of Omission, Producer and user accuracy for each classified category. Filling of this matrix is a necessity for this study since it focuses on accuracy improvement of classification resulting from fused image of Sentinel 1 and Sentinel 2.

Kappa Coefficient is a measure of the overall accuracy of classification taking into account the agreement occurring by chance. Error of commission gives the percentage of extra pixels in each class. Error of Omission gives the percentage of pixel left out from the class. Producer accuracy show the ratio of correctly classified pixel according to classifier and user accuracy's the ratio of matched ground truth with the classifier labels.

In the next chapter the results of confusion of the two case studies; France – Nice and Spain Zaragoza; are presented and the output of the classification.

The Final Overall procedure of the methodology undertaken in the delineation of the flood in my thesis is shown below in figure 29.

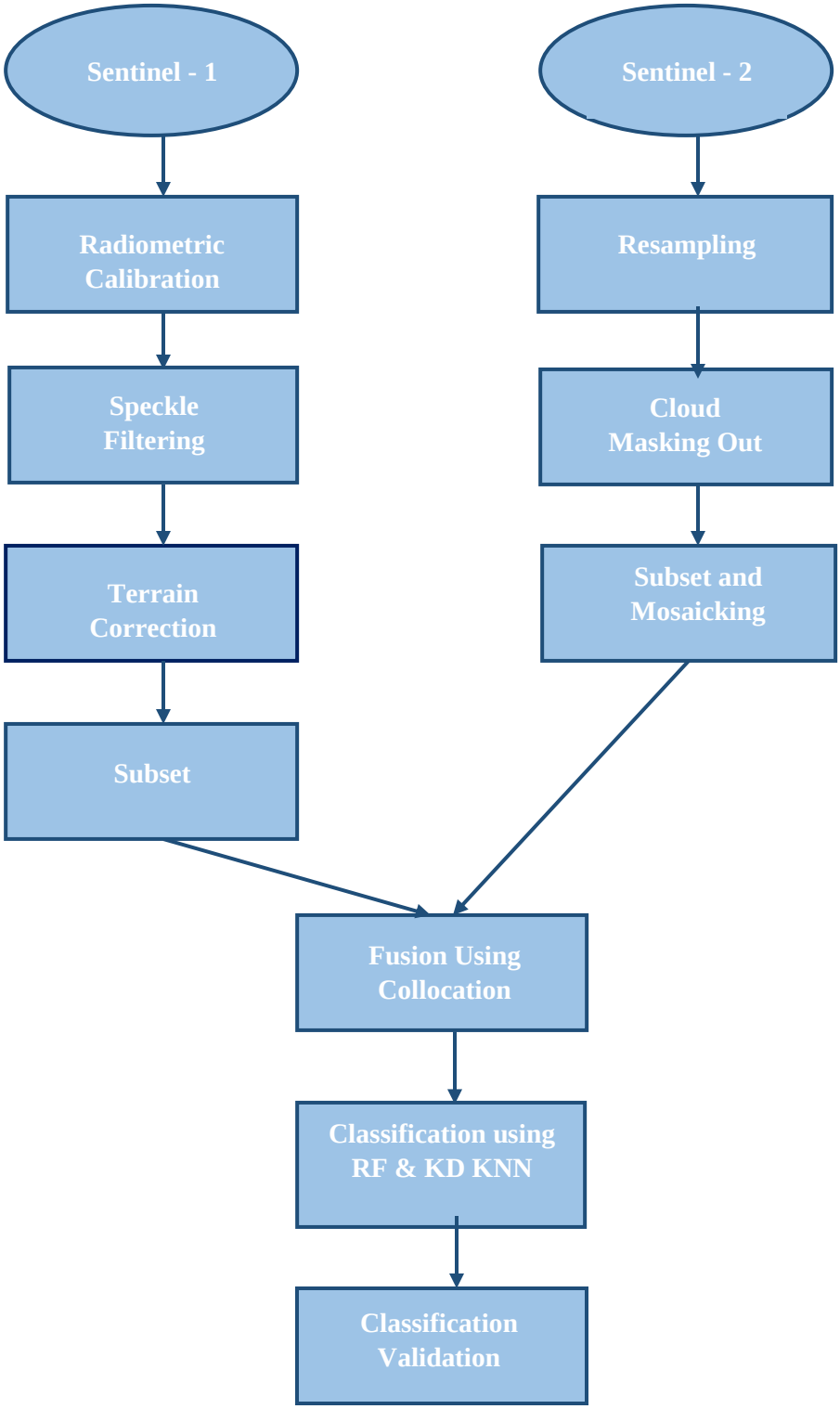

Figure 29:Overall Workflow of preprocessing and Processing

6. RESULTS AND CONCLUSION

This chapter presents the results and discussion of the generated output and accuracy. This chapter describes the results obtained through the previously described methods from case studies and formulates answers to the research objectives introduced in section 1.4.

6.1. RESULTS OF SPAIN ZARAGOZA CASE STUDY

Output of the processes done in the methodology is divided mainly into 3 Outputs: -

- Map of Fused Image (figure 30)
- Maps of Supervised Classification
    - Random Forest Supervised Classification (figure 32)
    - KD KNN Supervised Classification (figure 33)
- Confusion Matrix
    - Random Forest Confusion Matrix (Table 9)
    - KD KNN Confusion Matrix (Table 10)

Below is a demonstration of the above mentioned about, additionally the reference map (figure 31) that helps in identifying the accuracy of the outputs.

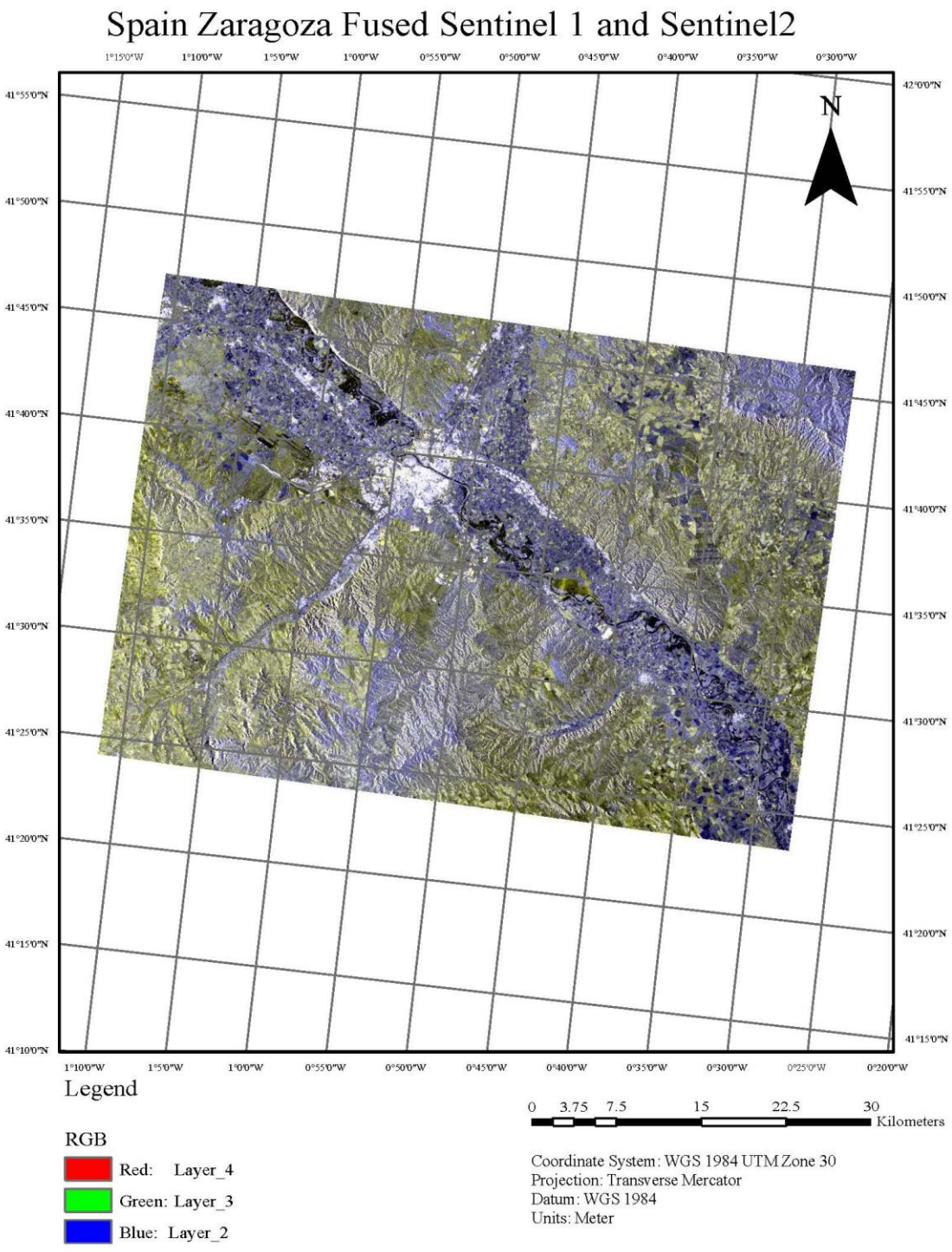

Figure 30: Spain Zaragoza Fused Sentinel 1 and Sentinel 2 Map

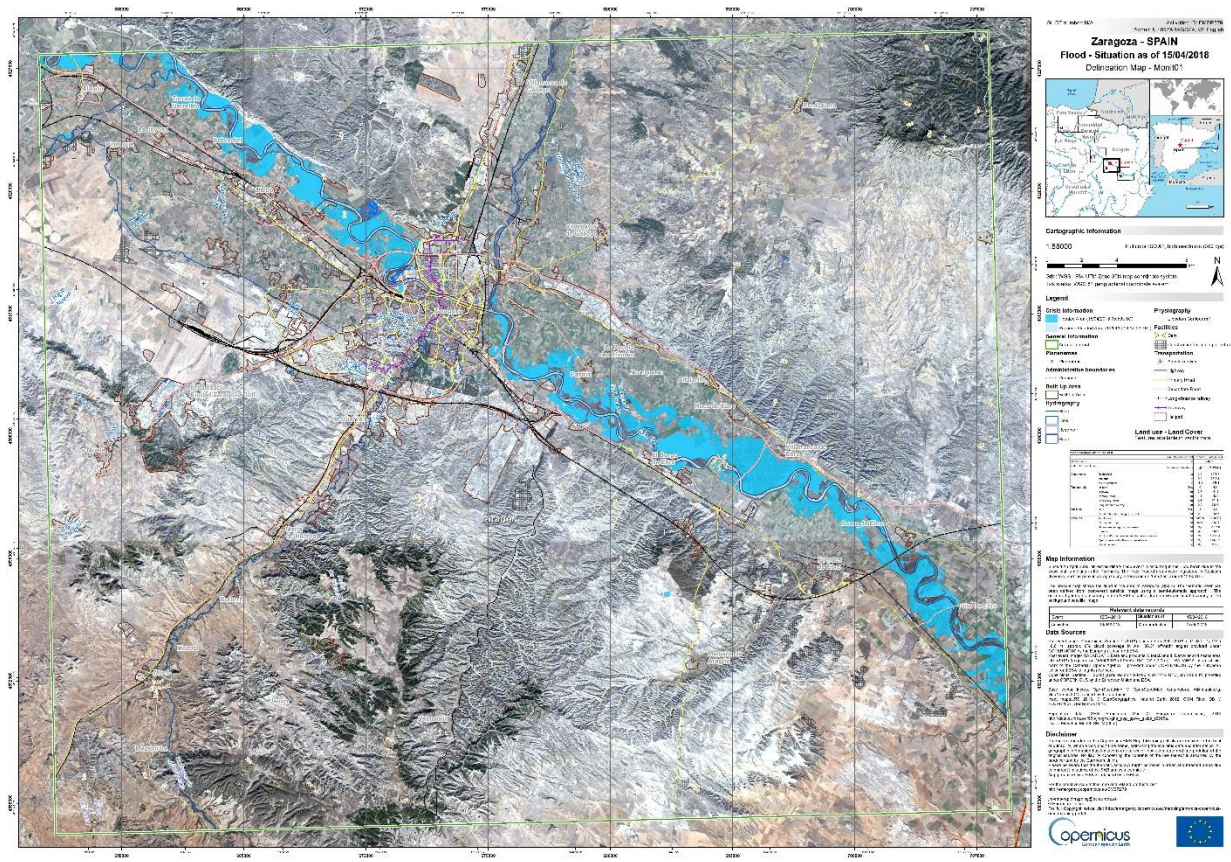

Figure 31:Spain Zaragoza Reference map from Copernicus (COPERNICUS_ European Commission, 2018)

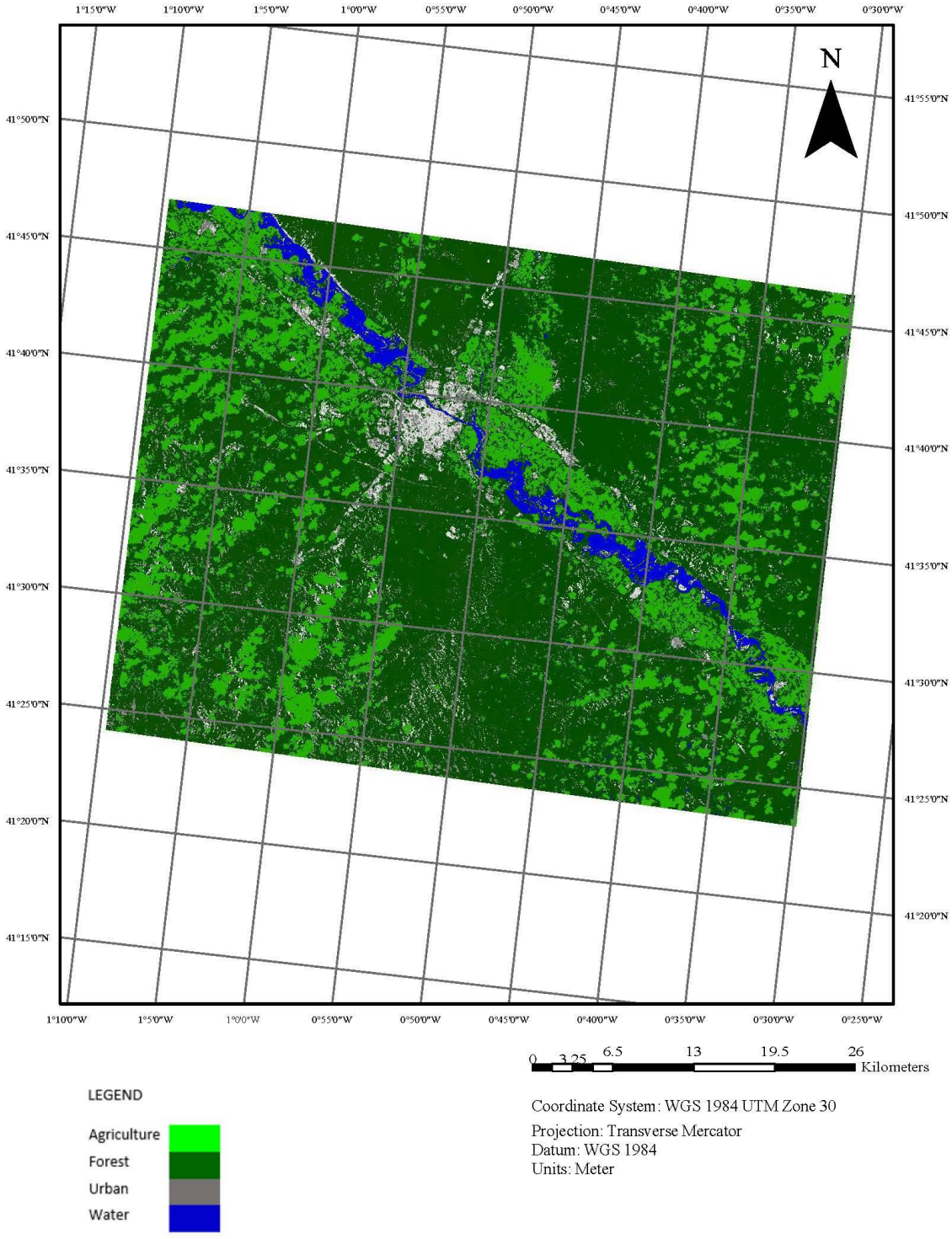

Figure 32:Spain Zaragoza Random Forest Supervised Classification

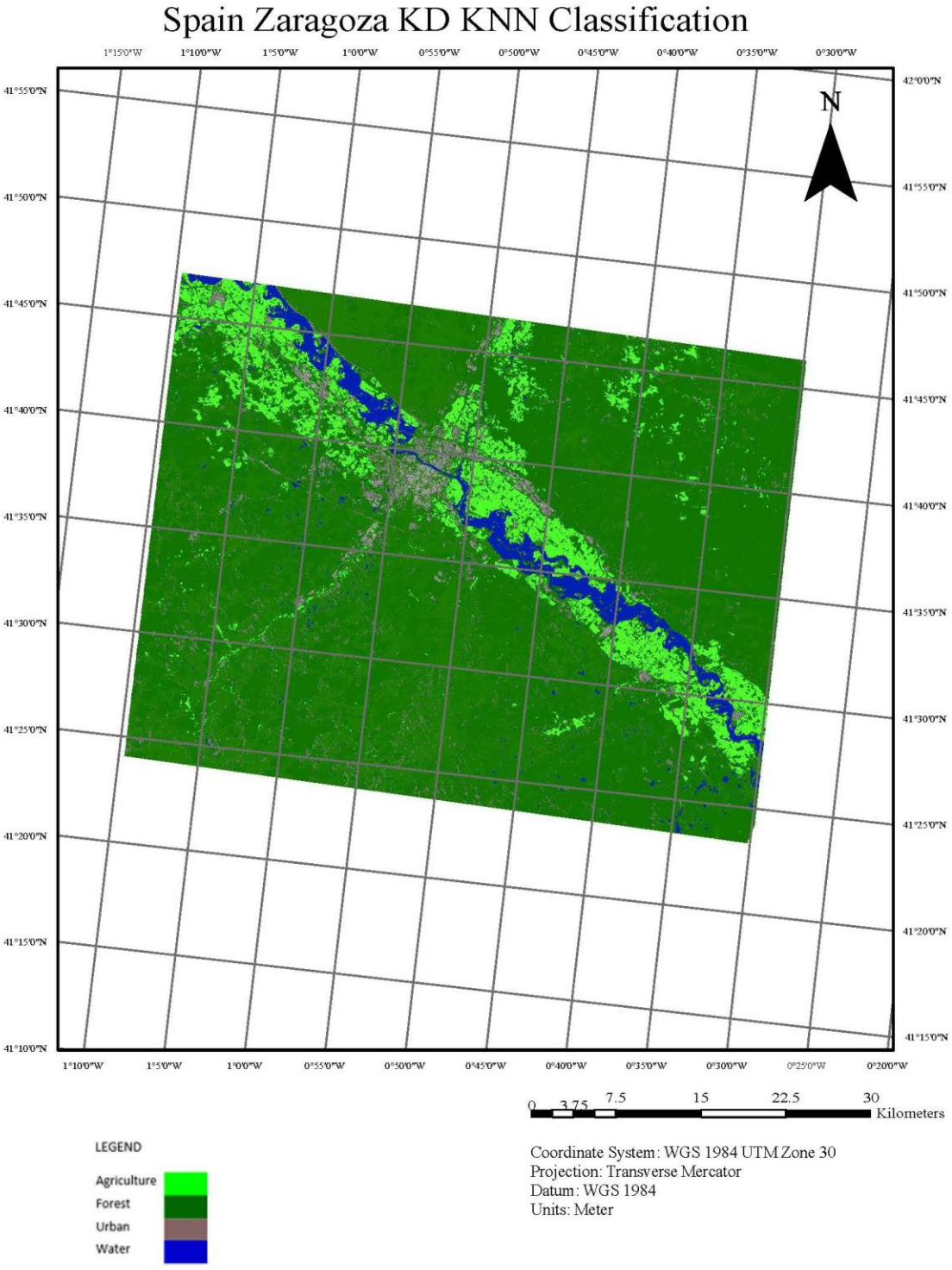

Figure 33:Spain Zaragoza KD KNN Supervised Classification

Land Cover Class	Relative to Copernicus Map		Relative to Fused Sentinel 1 and Sentinel 2	
	Producer Accuracy	User Accuracy	Producer Accuracy	User Accuracy
Agriculture	87.88%	78.38%	87.50%	100%
Forest	75%	68.18%	88.89%	81.63%
Urban	71.43%	83.33%	92.59%	86.21%
Water	90.24%	97.37%	100%	100%
Overall Accuracy	81.208%		92.83%	
Kappa Coeff.	0.749		0.904	

Table 9: Comparison of Producer's and User's Accuracy With Copernicus reference map and Fused image using Random Forest method

Land Cover Class	Relative to Copernicus Map		Relative to Fused Sentinel 1 and Sentinel 2	
	Producer Accuracy	User Accuracy	Producer Accuracy	User Accuracy
Agriculture	100%	100%	100%	100%
Forest	69.57%	88.89%	66.67%	95.65%
Urban	91.43%	71.11%	95.65%	66.67%
Water	97.44%	97.44%	100%	100%
Overall Accuracy	88.079%		90.08%	
Kappa Coeff.	0.841		0.868	

Table 10:Comparison of Producer's and User's Accuracy with Copernicus map and Fused image using KDKNN method

The results in the confusion matrix show that there is misinterpretation between forest and urban classes in the classification output of Random Forest as well as KD KNN methods relative to both Copernicus reference map *(Joint Research Centre Data Catalogue, 2018)* as well as in the fused image, however, there is an improvement in the results of the fused image as compared to Copernicus Reference map.

However, the Intercomparison relative to the fused image using both Random Forest and KD KNN methods shows 100% User and Producer accuracy in the water class. With an Overall accuracy in the Random Forest method of 92.83% and Kappa Coefficient of 0.904 and using KD KNN method of 90.08% overall accuracy and Kappa Coefficient of 0.868.

The Intercomparison relative to the Copernicus Reference map using Random Forest method shows 97.436%User and 90.24% Producer accuracy and 97.44% User and Producer accuracy using KD KNN in the water class. With an Overall accuracy in the Random Forest method of 81.208% and Kappa Coefficient of 0.749 and using KD KNN method of 88.079%overall accuracy and Kappa Coefficient of 0. 841. Surprisingly the accuracy results of intercomparison relative to reference is less for Random Forest method than in KD KNN. Table 7 shows the producer and user accuracy using Random Forest method and following Table 8 shows a comparison between producer and user accuracy using KD KNN method.

The results of Comparison show an improvement in the classification results of both methods Random Forest and KD-KNN when the Fused image of Sentinel 1 and Sentinel 2 images are used.

The Classification using Random Forest shows an over estimation in Agriculture class as compared to KDKNN. The Urban area surrounding the Ebro river is accurately mapped using both Random Forest and KD KNN as well as Agriculture field around the Ebro River. However, for the area away from the river where a lot of factors interfer and visual interpretation is unclear errors occurred in the classification factos such as clouds, shadow, sun and others play a role in misinterpretation and confusion. Most of the exaggerated Agriculture in Random Forest were mostly areas where clouds where located and removed.

6.2. RESULTS OF FRANCE NICE CASE STUDY

Output of the processes done in the methodology is divided mainly into 3 Outputs: -

- Map of Fused Image (figure 34)
- Maps of Supervised Classification
    - Random Forest Supervised Classification (figure 36)
    - KD KNN Supervised Classification (figure 37)
- Confusion Matrix
    - Random Forest Confusion Matrix (Table 11)
    - KD KNN Confusion Matrix (Table 12)

Below is a demonstration of the above mentioned about, additionally the reference map (figure 35) that helps in identifying the accuracy of the outputs.

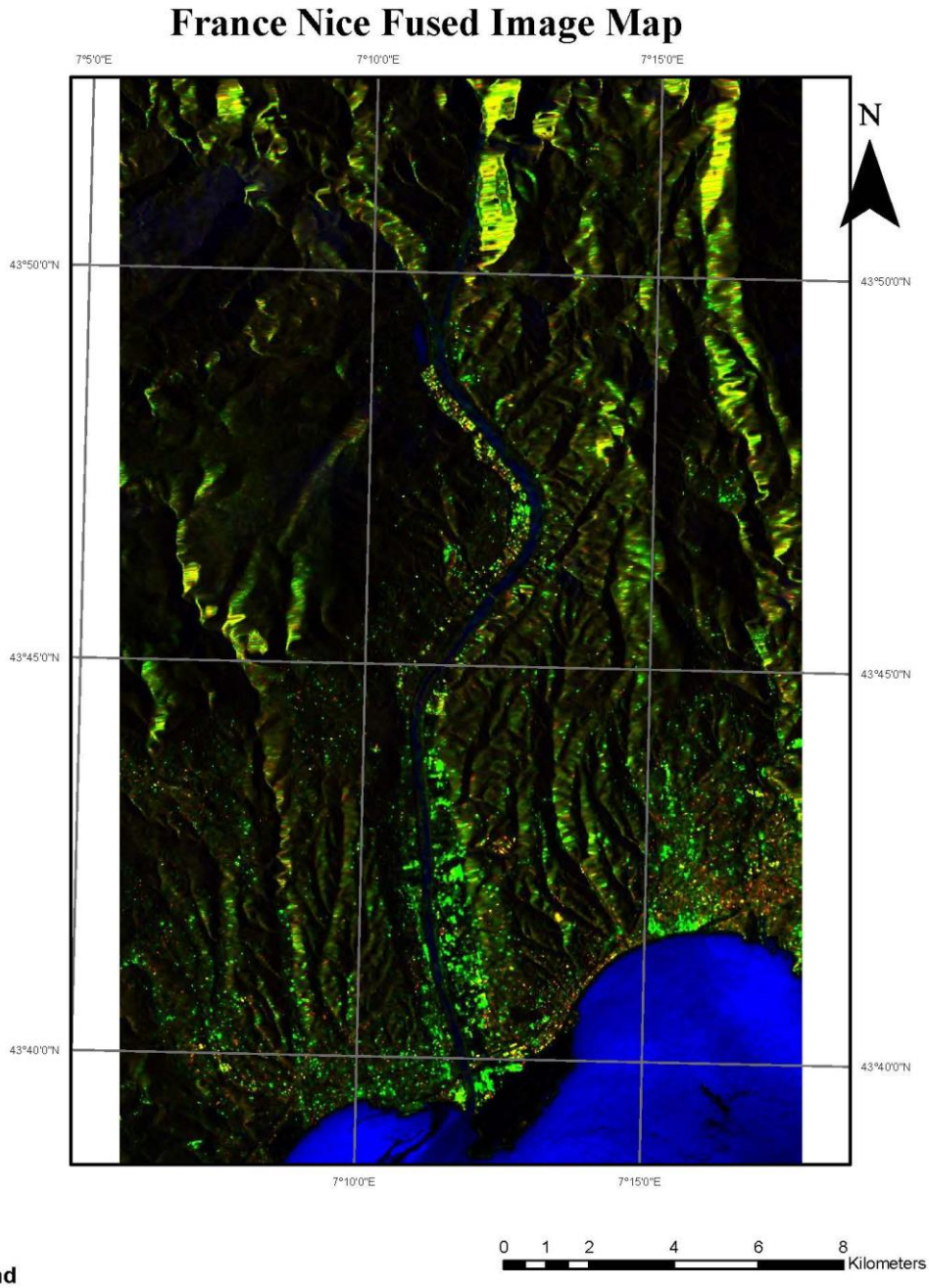

Figure 34:France Nice Fused Sentinel 1 and Sentinel 2 Map

Figure 35:France Nice Reference map from Copernicus (European Commission, Joint Research Centre, 2020)

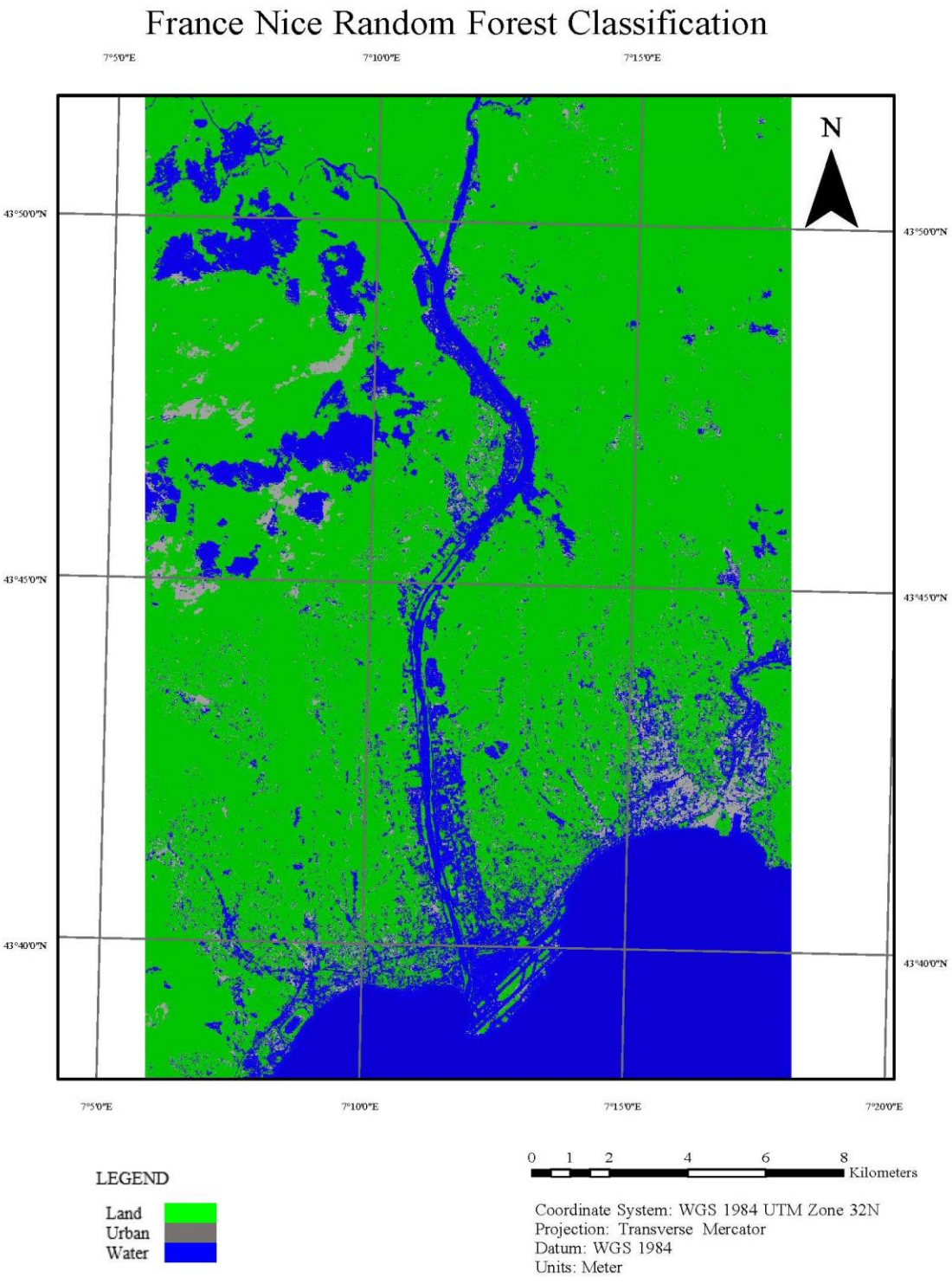

Figure 36:France Nice Random Forest Supervised Classification

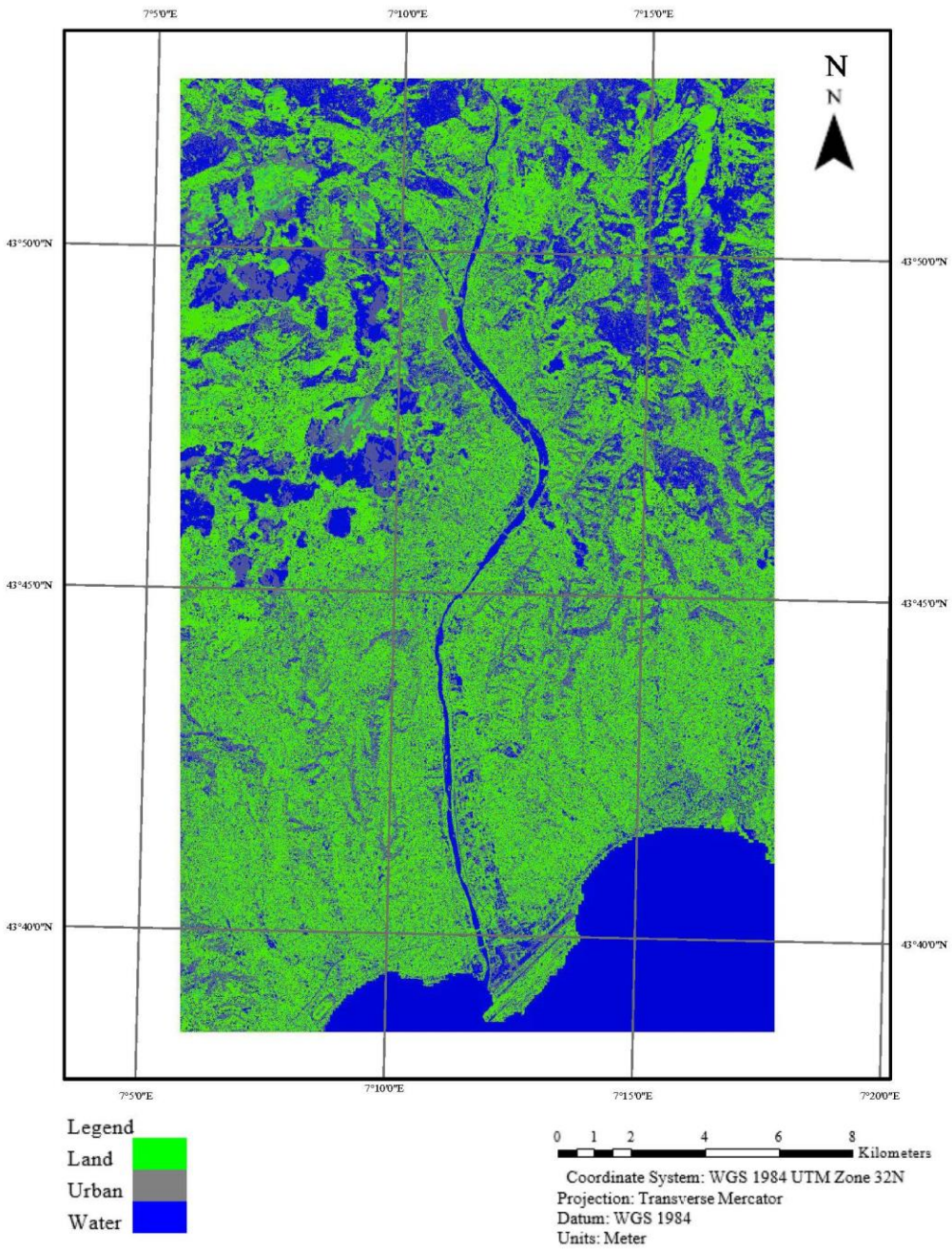

Figure 37:France Nice KD KNN Supervised Classification

Land Cover Class	Relative to Copernicus Map		Relative to Fused Sentinel 1 and Sentinel 2	
	Producer Accuracy	User Accuracy	Producer Accuracy	User Accuracy
Land	65.08%	78.85%	84.21%	100%
Urban	68.75%	80.49%	90.91%	81.08%
Water	85.71%	72.41%	91.30%	87.50%
Overall Accuracy	75.60%		88.89%	
Kappa Coeff.	0.606		0.832	

Table 11:Comparison of Producer's and User's Accuracy with Copernicus map and Fused image using RF method

Land Cover Class	Relative to Copernicus Map		Relative to Fused Sentinel 1 and Sentinel 2	
	Producer Accuracy	User Accuracy	Producer Accuracy	User Accuracy
Land	50%	69.23%	73.33%	68.75%
Urban	60.87%	68.29%	67.5%	62.79%
Water	79.12%	62.07%	72%	80%
Overall Accuracy	65.07%		70.83%	
Kappa Coeff.	0.445		0.556	

Table 12:Comparison of Producer's and User's Accuracy with Copernicus map and Fused image using KD KNN method

The results in the confusion matrix shows that there is misinterpretation between water and urban classes in the classification output of Random Forest as well as KD KNN methods relative to both Copernicus reference map (Joint Research Centre Data Catalogue, 2020) as well as in the fused image, however, there is an improvement in the results of the fused image as compared to Copernicus Reference map for Random Forest, unlike the case study of Spain the Random Forest method showed better results than KD KNN also the KD KNN results for both the Copernicus reference map (Joint Research Centre Data Catalogue, 2020) as well as in the fused image were not very good.

However, the Intercomparison relative to the fused image using Random Forest methods shows 87.5% User and 91.3% Producer accuracy in the water class and for KD KNN methods shows 80% User and 72% Producer accuracy in the water class. With an Overall accuracy in the Random Forest method of 88.89% and Kappa Coefficient of 0.832 and using KD KNN method of 70.83% overall accuracy and Kappa Coefficient of 0.556.

The Intercomparison relative to the Copernicus Reference map using Random Forest method shows 72.414% User and 85.714% Producer accuracy and 62.069% User and 79.121% Producer accuracy using KD KNN in the water class. With an Overall accuracy in the Random Forest method of 75.60%and Kappa Coefficient of 0.606 and using KD KNN method of 65.07% overall accuracy and Kappa Coefficient of 0.445. Table 9 shows the producer and user accuracy using Random Forest method and following Table 10 shows a comparison between producer and user accuracy using KD KNN method.

The results of Comparison show an improvement in the classification results of Random Forest method when the Fused image of Sentinel 1 and Sentinel 2 images are used.

6.3. CONCLUSION

Flood risk mapping is an essential component for relevant land use planning in flood plain areas and it aids in the efforts of city planners and administrators to prioritize their mitigation or relief response. The basic notion of flood risk mapping undertaken in this thesis is to efficiently delineate flood prone areas in the selected study cases of Spain Zaragoza and France Nice.

The goal of this thesis was to perform an operational mapping of the flooding using the synergic fusion SAR and optical images in a minimum of time, and ideally in an automatic way. Free satellite data of Sentinel 1 and Sentinel 2 was preferred to make the introduced algorithms accessible to any region prone to flooding, regardless of its geographical location and its budget as well as and the SNAP Tool of ESA which are freely available providing the sufficient means for this thesis purpose. Two algorithms of Supervised classification; Random Forest and KD KNN; processes were presented where the interest was identifying and in mapping the extent of the flood from the fused images.

This process proved capable of a quick and automatic mapping of the extent of the inundation, which can assist response authorities to prioritize during rescue operations through experimental results. The rapidity of execution is a very important factor especially when the main purpose of the flood map is to support relief efforts at the time of the disaster. This approach was evaluated on two flood events Spain Zaragoza and France Nice captured by Sentinel 1 and Sentinel 2.

According to the assessment metrics calculated to evaluate the accuracy of the classification, the results were reasonable for France Nice and more accurate for Spain Zaragoza, considering that the technique and quality of images used for the fused Sentinel 1 and Sentinel 2, and the images used for the intercomparison map of Copernicus were different. The Copernicus Reference maps presented were mainly created using single imagery source either SAR imagery or Optical imagery. The Intercomparison relative to Copernicus Reference map (single source data) proved that using the fused image of SAR and Optical developed higher accuracy specifically in water class.

Results show that for Spain Zaragoza using Random Forest supervised classification Kappa Coefficient was 0.904 with a 100% producer and user accuracy for the Water class and an overall accuracy of 92.83% and using KD KNN results show Overall accuracy of 90.08, Kappa Coefficient of 0.868 even though decreased the producer and user accuracy for the Water class is still 100%.

For France Nice Overall accuracy in Random Forest show an 88.89% and Kappa Coefficient of 0.832 with a 91.30% producer and 87.50% user accuracy for the Water class and using KD KNN an overall accuracy 70.83 and Kappa Coefficient of 0.556 with a 72% producer and 80% user accuracy for the Water class. Both cases proved better results in intercomparison with Copernicus map single imagery source

Flood maps derived from remotely sensed images are always, although to different extents, affected by errors, no matter what type of images and which pattern recognition algorithm have been used. The training data required by the supervised classification method were delineated manually on the optical dataset. The accuracy of the work presented can be further improved by using higher resolution data which will generate flood inundation map with higher accuracy.

Fusing SAR and Optical Images was of advantage because both the sources complimented each other. SAR sensor using microwave to penetrate returning a backscatter rich with data regardless of the weather condition and the importance of Multispectral optical image to identify feature on the surface thus being able to define a training sample that is to be used in classification and carrying data for clouds free regions that are useful in determining more accurately the class of the pixels, a fused image is having more bands to help improving the accuracy and results of classification. However, there are still limitations due to Sentinel 1 and Sentinel 2 resolution. Using higher resolution would have further helped in improving the output, as well as, having ground truth would have helped the evaluation of the results. Another limitation is that after removing the clouds from the Optical image the pixels are given a No Data Value therefore, in this case the classification relies only on SAR image for pixel value returning to the idea that a single source is still used in clouded areas of the image.

Future work improvements that can be carried out include: -

- The flood extent classifier showed satisfying results on the datasets examined, however it might fail if the water bodies and rivers are too small to appear clearly in the pre-flood Sentinel 1 and the Sentinel-2 product. In this particular case, the classifier cannot be trained efficiently to recognize the water class. In the future, the method proposed to delineate the extent of the inundation could benefit from recent commercial optical sensors, capable of delivering metric or even sub-metric resolution images, to address the above-mentioned issue concerning narrow river channels that cannot be distinguished with the 10 m-resolution Sentinel-1 and Sentinel-2.

- Looking more in depth into adapting and applying the inundation extent mapping algorithm to urban areas, since they are at a higher risk of human and financial losses.

- Detecting and delimitating non-permanent from permanent water surfaces from Fused images and other classes as well however this mainly depends on two parameters. First the use of higher resolution imagery to identify other classes. Secondly, having other input such as vector layer for the main layers for example roads, rivers, lakes, agriculture fields with their types.

- Finally, Obtaining Ground truth and field data that could be used to better check the accuracy of the results.

7. REFERENCES

Blöschl, G. et al. 2019. *Changing climate both increases and decreases European river foods. Nature 573, 108–111 .* 2019.

Githeko, A. & Ndegwa, W. 2001. *Predicting malaria epidemics in the Kenyan highlands using climate data: a tool for decision-makers. Global Change & Human Health.* 2001.

AFP/The Local. 2020. 2020.

Alberto Refice, Annarita D'Addabbo,Domenico Capolongo. 2017. *Flood Monitoring through Remote Sensing.* 2017.

Amarsaikhan, D., & Douglas, T. 2004. *Data Fusion and multisource image classification.* s.l. : International Journal of Remote Sensing, 2004.

António Guterres, Secretary-General of the United Nations. 2021. s.l. : World Meteorological Organization (WMO), 2021.

Balzter, H., Cole, B., Thiel, C., and Schmullius, C. 2015. *Mapping CORINE Land Cover from Sentinel-1A SAR and SRTM Digital Elevation Model Data using Random Forests.* 2015.

Ban, H.-J., et al. 2017. *Flood monitoring using satellite-based RGB composite imagery and refractive index retrieval in visible and near-infrared bands.* 2017.

BBC. *Storm Alex: Floods and landslides hit France and Italy.*

Behnamian, A. , Banks, S. , White, L. , Brisco, B. , Milard, K. , Pasher, J. , … Battaglia, M. 2017. *Semi-automated surface water detection with synthetic aperture radar data: A Wetland case study. Remote Sensing.* 2017. 9(12), 1209. doi:10.3390/rs9121209.

Berz, G., Kron, W., Loster, T. et al. World Map of Natural Hazards – A Global View of the Distribution and Intensity of Significant Exposures. Natural Hazards 23, 443–465 (2001). 2001. 2001.

Beste Tavus, Sultan Kocaman, Hakan A. Nefeslioglu, Candan Gokceoglu. 2020. *A FUSION APPROACH FOR FLOOD MAPPING USING SENTINEL-1 AND SENTINEL-2 DATASETS.* 2020.

Beste Tavus1, Sultan Kocaman1, *, Hakan A. Nefeslioglu2, Candan Gokceoglu2. 2020. *A FUSION APPROACH FOR FLOOD MAPPING USING SENTINEL-1 AND SENTINEL-2 DATASETS.* 2020.

Bioresita, F., et al. 2018. *method for automatic and rapid mapping of water surfaces from Sentinel-1 imagery.* 2018.

Björn Waske, Associate Member, IEEE, and Sebastian van der Linden. 2008. *Classifying Multilevel Imagery From SAR and Optical Sensors by Decision Fusion.* 2008.

—. 2008. *Classifying Multilevel Imagery From SAR and Optical Sensors by Decision Fusion.* 2008.

Boni, G., Pierdicca, N., Pulvirenti, L., Squicciarino, G., and Candela, L. 2015. *Joint Use Of X- And C-band SAR Images For Flood Monitoring : The 2014 Po River Basin Case Study.* s.l. : IEEE International Geoscience and Remote Sensing Symposium (IGARSS), 2015.

Breiman, L.,. 2001. *Random forests. Machine Learning.* 2001.

Byun, Y., Han, Y., & Chae, T. 2015. *Image fusion-based change detection for flood extent extraction using bi-temporal very high-resolution satellite images.* 2015.

Campbell and Wynne. 2011. *Introduction to Remote Sensing Fifth Edition.* 2011.

Campbell, J. B. and Wynne, R. H. 2011. *Introduction to remote sensing.* s.l. : Guilford, 2011.

Chaouch, Naira, et al. 2011. *A synergetic use of satellite imagery from SAR and optical.* 2011.

Christodoulou A., Demirel H. 2018. *Impacts of climate change on transport .* s.l. : European Commission, 2018.

CNN. 2020. *France and Italy floods.* 2020.

Cohen, M., Larkins, A., Semedo, P. L., and Burbidge, G. 2017. *Novasar-s low cost spaceborne sar payload design, development and deployment of a new benchmark in spaceborne radar.* s.l. : IEEE Radar Conference, 2017.

COMMISSION STAFF WORKING. 2021. *Commission Staff Working Document, Adapting infrastructure to climate change. Forging a climate-resilient Europe - The new EU Strategy on Adaptation to Climate.* Brussel : s.n., 2021.

CONFEDERACIÓN HIDROGRÁFICA DEL EBRO COMISARIA DE AGUAS. 2018. *MINISTERIO DE AGRICULTURA Y PESCA, ALIMENTACIÓN Y MEDIO AMBIENTE.* 2018.

Confederación Hidrográfica del Ebro, CHE. 2018. *Ministerio Para la Transición Ecológica; Gobierno de España. Ministerio Para la Transición Ecológica; Gobierno de España.* 2018.

COPERNICUS_ European Commission. 2018. *Flood in the Ebro river basin, Spain.* 2018.

Dabrowska-Zielinska, K., et al. 2014. *Monitoring wetlands ecosystems using ALOS PALSAR (L-Band, HV) supplemented by optical data: A case study of Biebrza Wetlands in Northeast Poland.* 2014.

David P. Roy, Jian Li,Hankui K. Zhang & Lin Yan. 2016. *Best practices for the reprojection and resampling of Sentinel-2 Multi Spectral Instrument Level 1C data.* 2016.

de Leeuw, M. R. and de Carvalho, L. M. T. 2009. *Performance evaluation of several adaptive speckle filters for sar imaging. Anais XIV Simp´osio Brasileiro de Sensoriamento Remoto.* 2009. pp. 7299–7305.

Deutsch, M. and Ruggles, F. 1974. *Deutsch, M. and Ruggles, F. (1974). Optical Data Processing and Projected Applications.* 1974.

Drusch, M. et al.,. 2012. *Sentinel-2: ESA's Optical High-Resolution Mission for GMES Operation Service.Remote Sensing of Environment.* 2012.

EEA. 2011. *"Mapping the impacts of natural hazards and technological accidents in Europe".* 2011.

—. 2010. *: The European Environment, State and Outlook 2010.Water Resources: Quantity and Flows.* 2010.

—. 2012. *Climate Change, Impacts and Vulnerability in Europe 2012.* 2012.

Ehlers, M. 1991. *Multisensor image fusion techniques in remote sensing.* s.l. : ISPRS Journal of Photogrammetry and Remote Sensing, 1991.

—. 2004. *Spectral characteristics preserving image fusion based on Fourier domain filtering. Remote Sensing for Environmental Monitoring, GIS Applications, and Geology IV.* 2004.

ESA. *Flood monitoring.*

Estel, S., Kuemmerle, T., Alcántara, C., Levers, C., Prishchepov, A., & Hostert, P. 2015. *Mapping farmland abandonment and recultivation across Europe using MODIS NDVI time series. Remote Sensing of Environment.* 2015.

European Commission. 2007. *Directive 2007/60/EC of the European Parliament and of the Council the assessment and management of flood risks.* s.l. : Official Journal of the European Union, vol. L288, 2007.

EUROPEAN COMMISSION. 2014. *Guide to Cost-Benefit Analysis.* 2014.

—. 2018. *IN-DEPTH ANALYSIS IN SUPPORT OF THE COMMISSION.* Brussels : s.n., 2018.

European Commission, Joint Research Centre. 2020. *Flood in Alpes-Maritimes, France (2020-10-03).* 2020.

European Parliament. 2007. *Directive 2007/60/EC of the European Parliament and of the Council of 23 October 2007 on the assessment and management of flood risks.* 2007.

Fabrizio_Ramoino, marpet. 2017. *Layer stackin in SNAP for Sentinel 2.* 2017.

Feyen, et al. 2016. *Increasing flood risk under climate change: a pan-European assessment of the benefits of four adaptation strategies. Climatic Change .* 2016.

Flood List. 2018. *FloodList - Reporting floods and flooding news.* 2018.

Gérard Biau, Erwan Scornet. 2015. *A_Random_Forest Guided Tour.* 2015.

Gholizadeh, M., Melesse, A. & Reddi, L.,. 2016. *A Comprehensive Review on Water Quality Parameters Estimation Using Remote Sensing Techniques. Sensors.* 2016.

Green, A. A. 2007. *Green, A. A., Whitehouse, G., and Outhet, D. (2007). Causes of Flood Streamlines.* 2007.

Guha-Sapir, D., Hoyois, P., and Below, R. 2015. *Annual Disaster Statistical Review 2014: The Numbers and Trends. Brussels: CRED.* Brussels : s.n., 2015.

Henry, J.-B., et al. 2006. *Envisat multipolarized ASAR data for flood mapping.* 2006.

Hong, Y., Adhikari, P., and Gourley, J. J. 2013. *Flood Hazard and Disaster. In Bobrowsky, P. T., editor, Encyclopedia of Natural Hazards, Encyclopedia of Earth Sciences Series.* Netherlands, Dordrecht : s.n., 2013.

Horvat, Bacc.ing.tech.inf. Zlatko. 2012. *CHANGE DETECTION IN LAND USE LAND COVER (LULC) IN MEĐIMURJE COUNTY, CROATIA, BETWEEN 1978, 1992 AND 2007 USING LANDSAT SATELLITE IMAGERY.* UNIGIS MSc programme at the Centre for GeoInformatics (Z_GIS), Salzburg University. 2012. p. 6.

Intera Kenting Ltd. 1992. *REMOTE SENSING TO MONITOR URANIUM TAILING SITES .* Ottawa, Canada : Atomic Energy Control Board, 1992.

Irwin, K. , Beaulne, D. , Braun, A. , & Fotopoulos, G. 2017. *Fusion of SAR, optical imagery and airborne LiDAR for surface water detection. Remote Sensing ,.* 2017. 10.3390/rs9090890.

Jiri Marsalek, Gheorghe Stancalie,Gabor Balint. 2006. *Transboundary Floods: Reducing Risks Through Flood Management.* National Water Research Institute. 2006.

Joint Research Centre Data Catalogue. 2020. *Flood in Alpes-Maritimes, France (2020-10-03).* 2020.

—. 2018. *Title: Flood in the Ebro river basin, Spain (2018-04-13).* s.l. : Copernicus, 2018.

JRC PESETA IV. 2020. *Climate change impacts and adaptation in Europe .* 2020.

Kríz, B. 1998. *Infectious diseases: consequences of the massive 1997 summer flood in the Czech Republic.* 1998.

Larrue C, Bruzzone S, Lévy L, et al. 2016. *Analysing and evaluating ood risk governance in France. From state policy to local strategies.* 2016.

Lee, W. J., Lu, Z., Jung, H. S., and Ji, L. . 2017. *Measurement of small co-seismic deformation field from multi-temporal SAR interferometry: application to the 19 September 2004 Huntoon Valley earthquake.* 2017.

Lillesand, T.M., Kiefer, R.W. & Chipman, J.W.,. 2008. *Remote Sensing and Image Interpretation 6th edition.* 2008.

Mangolini, M. 1994. *Apport de la fusion d'images satellitaires multicapteurs au niveau pixel en télédétection et photointerprétation.* s.l. : Université de Nice Sophia-Antipolis, Nice, France, 1994.

Map-France.com. *Map-France.com.*

Martinis, S. and Rieke, C. 2015. *Backscatter analysis using multi-temporal and multi-frequency SAR data in the context of flood mapping at river Saale.* 2015.

Mason, D., Giustarini, L., Garcia-Pintado, J., and Cloke, H. 2014. *Detection of flooded urban areas in high resolution Synthetic Aperture Radar images using double scattering.* 2014.

Melpomeni Zoka *, Emmanouil Psomiadis and Nicholas Dercas. 2018. *The Complementary Use of Optical and SAR Data in Monitoring Flood Events and Their Effects.* 2018.

Melrose, R. T., Kingsford, R. T., and Milne, a. K. 2012. *Using radar to detect flooding in arid wetlands and rivers.* s.l. : 2012 IEEE International Geoscience and Remote Sensing, 2012.

Messner, F. 2007. *Evaluating flood damages: guidance and recommendations on principles and methods.* 2007.

Morris Deutsch Fred Ruggles. 1974. *OPTICAL DATA PROCESSING AND PROJECTED APPLICATIONS OF THE ERTS-1 IMAGERY COVERING THE 1973 MISSISSIPPI RIVER VALLEY FLOODS.* 1974.

N. Anusha, B. Bharathi. 2019. *Flood detection and flood mapping using multi-temporal synthetic aperture radar and optical data.* 2019.

NatCatSERVICE. 2017. *Data on natural disasters since 1980. Munich Re.* 2017.

Nath, R.K. & Deb, S.K., 2010. *Water-Body Area Extraction From High Resolution Satellite Images-An Introduction, Review, and Comparison. International Journal of Image Processing.*

Niklas Donges. 2020. *A COMPLETE GUIDE TO THE RANDOM FOREST ALGORITHM.* 2020.

Otair, Dr. Mohammed. 2013. *APPROXIMATE K-NEAREST NEIGHBOUR BASED SPATIAL CLUSTERING USING K-D TREE.* Department of Computer Information Systems, Amman Arab University. Amman, Jordan : International Journal of Database Management Systems (IJDMS), 2013.

Ozdemir, C. 2012. *Inverse Synthetic Aperture Radar Imaging with MATLAB Algorithm.* UNITED STATES : John Wiley & Sons, Incorporated, Hoboken, 2012.

P¨uschel, J. 2005. *Risk factor of water: Special feature issue. .* MunichRe : s.n., 2005.

Padmanabhan, S. B. Gurjar & N. 2005. *Study of various resampling techniques for high-resolution remote sensing imagery.* s.l. : Journal of the Indian Society of Remote Sensing volume, 2005.

Paprotny D, Sebastian A, Morales-Nápoles O, Jonkman SN. 2018. *Trends in flood losses in Europe over the past 150 years.* 2018.

Parmenter, R.R. et al. 1999. *Incidence of plague associated with increased winter-spring precipitation in New Mexico.* s.l. : American Journal of Tropical Medicine and Hygiene, 1999.

Patz, J.A. et al. 1998. *Predicting key malaria transmission factors, biting and entomological inoculation rates, using modelled soil moisture in Kenya.* s.l. : Tropical Medicine and International Health, 1998. (10): 818–827.

Planatek Italia. 2019. *The History of Remote Sensing.* 2019.

Podest. 2017. *Basics of synthetic aperture radar (sar).* 2017.

Podlaha, A., L¨orinc, M., Bowen, S., and Bhattacharya, A. 2019. *Weather, climate & catastrophe insight - 2018 annual report.* 2019.

Pohl, C., & Van Genderen, J.L. 1998. *Review article multisensor image fusion in remote sensing: Concepts, methods and applications.* s.l. : International Journal of Remote Sensing, 1998.

Qiu, F., Berglund, J., Jensen, J. R., Thakkar, P., and Ren, D. 2004. *Speckle noise reduction in sar imagery using a local adaptive median filter.* 2004.

R.S., R. Valentini, L.M. Bouwer, E. Georgopoulou, D. Jacob, E. Martin, M. Rounsevell, and J.-F. Soussana. 2014. *Europe : In: Climate Change 2014: Impacts, Adaptation, and Vulnerability.* 2014.

Raspini, F., Ciampalini, A., Del Conte, S., Lombardi, L., Nocentini, M., Gigli, G.,. 2015. *Exploitation of amplitude and phase of satellite SAR images for landslide mapping: The case of Montescaglioso (South Italy).* 2015.

Reddy, A. 2006. *Textbook of remote sensing and geographical information systems.* Hyderabad : BS Publications,, 2006.

2021. Remote Sensing Tool For Students and Teachers - Making a Subset. [Online] 2021. (https://sites.google.com/site/remotesensingtool/making-a-subset).

Roudier P, Andersson JCM, Donnelly C, et al,. 2016. *Projections of future □oods and hydrologicalnder under a +2°C global warming.* 2016.

S. Domenech, F. Espejo, A. Ollero, M. Sánchez-Fabre. 2009. *Recent floods in the Middle Ebro River, Spain: hydrometeorological aspects and floodplain management.* 2009.

Schowengerdt, R.A.,. 2007. *Remote Sensing: Models and Methods for Image Processing. Third Edition,.* 2007.

Schumann, G.J-P. Preface: Remote Sensing in Flood Monitoring and Management. Remote Sens. 2015, 7, 17013-17015. https://doi.org/10.3390/rs71215871. 2015. 2015.

Senthilnath, J., et al. 2013. *Integration of speckle de-noising and image segmentation using Synthetic Aperture Radar image for flood extent extraction.* 2013.

Simoes, J. et al. 1967. *Some aspects of the Weil's disease epidemiology based on a recent epidemic after a flood in Lisbon.* 1967.

SINGH, GURCHETAN. 2017. *Introductory guide to Information Retrieval using kNN and KDTree.* 2017.

Step Forum. 2017. *Cloud mask - SNAP sentinel 2.* 2017.

Sunuprapto, H., & Hussin, Y. A. 2000. *A comparison between optical and radar satellite images in detecting burnt tropical forest in south Sumatra, Indonesia.* 2000.

T. M. Lillesand, R. W. Kiefer and J. W. Chipman. 2008. *Remote sensing and image interpretation: 6th edition.* s.l. : Hoboken, NJ: John Wiley & Sons, 2008.

Tan, H. & NASA. 2016. *ASTER website.* 2016.

Tavus, B., et al. 2018. *Considerations on the use of Sentinel-1 data in flood mapping in urban areas.* Ankara (Turkey) : s.n., 2018.

THE EUROPEAN SPACE AGENCY. *Satellite Description.*

Ulaby, F., Long, D., Blackwell, W., Elachi, C., Fung, A., Ruf, C., Sarabandi, K.,. 2014. *Microwave Radar and Radiometric Remote Sensing.* s.l. : University of Michigan Press, 2014.

UNISDR, CRED. 1996 - 2015. *Poverty & Death: Disaster Mortality 1996-2015.* s.l. : UNISDR, CRED, 1996 - 2015.

VIDHYA, ANALYTICS. 2016. *Tree Based Algorithms: A Complete Tutorial from Scratch (in R & Python).* 2016.

Voormansik, K., Praks, J., Antropov, O., Jagomagi, J., and Zalite, K. 2014. *Flood mapping with terraSAR-X in forested regions in estonia.* s.l. : IEEE Journal, 2014.

WORLD HEALTH ORGANIZATION. 2003. *CLIMATE CHANGE AND HUMAN HEALTH.* Geneva : s.n., 2003.

World Meteorological Organization. 2013. *"Integrated Flood Management Tools Series No.20 flood mapping," Associated Programme on Flood Management.* Switzerland : s.n., 2013.

Zhong, S., Yang, L., Toloo, S., Wang, Z., Tong, S., Sun, X., Crompton, D., FitzGerald, G., and Huang, C. 2018. *The long-term physical and psychological health impacts of flooding: A systematic mapping. Science of the Total Environment,.* 2018.